SJSU SAN JOSÉ STATE UNIVERSITY

MTI MINETA TRANSPORTATION INSTITUTE

# Stability of Fiber-Reinforced Bridge Bearings under Compression and Shear Loads

Andrea Calabrese, PhD
Simone Galano
Nghiem Tran

CSUTC California State University Transportation Consortium

CALIFORNIA STATE UNIVERSITY LONG BEACH

CSU TRANSPORTATION CONSORTIUM

transweb.sjsu.edu/csutc

# MINETA TRANSPORTATION INSTITUTE

Founded in 1991, the Mineta Transportation Institute (MTI), an organized research and training unit in partnership with the Lucas College and Graduate School of Business at San José State University (SJSU), increases mobility for all by improving the safety, efficiency, accessibility, and convenience of our nation's transportation system. Through research, education, workforce development, and technology transfer, we help create a connected world. MTI leads the four-university. MTI leads the four-university California State University Transportation Consortium funded by the State of California through Senate Bill 1.

MTI's transportation policy work is centered on three primary responsibilities:

### Research

MTI works to provide policy-oriented research for all levels of government and the private sector to foster the development of optimum surface transportation systems. Research areas include: bicycle and pedestrian issues; financing public and private sector transportation improvements; intermodal connectivity and integration; safety and security of transportation systems; sustainability of transportation systems; transportation / land use / environment; and transportation planning and policy development. Certified Research Associates conduct the research. Certification requires an advanced degree, generally a Ph.D., a record of academic publications, and professional references. Research projects culminate in a peer-reviewed publication, available on TransWeb, the MTI website (http://transweb.sjsu.edu).

### Education

The Institute supports education programs for students seeking a career in the development and operation of surface transportation systems. MTI, through San José State University, offers an AACSB-accredited Master of Science in Transportation Management and graduate certificates in Transportation Management, Transportation Security, and High-Speed Rail Management that serve to prepare the nation's transportation managers for the 21st century. With the active assistance of the California Department of Transportation (Caltrans), MTI delivers its classes over a state-of-the-art videoconference network throughout the state of California and via webcasting beyond, allowing working transportation professionals to pursue an advanced degree regardless of their location. To meet the needs of employers seeking a diverse workforce, MTI's education program promotes enrollment to under-represented groups.

### Information and Technology Transfer

MTI utilizes a diverse array of dissemination methods and media to ensure research results reach those responsible for managing change. These methods include publication, seminars, workshops, websites, social media, webinars, and other technology transfer mechanisms. Additionally, MTI promotes the availability of completed research to professional organizations and journals and works to integrate the research findings into the graduate education program. MTI's extensive collection of transportation- related publications is integrated into San José State University's world-class Martin Luther King, Jr. Library.

REPORT 20-25

# STABILITY OF FIBER-REINFORCED BRIDGE BEARINGS UNDER COMPRESSION AND SHEAR LOADS

Andrea Calabrese, PhD
Simone Galano
Nghiem Tran

July 2020

A publication of
**Mineta Transportation Institute**
Created by Congress in 1991

College of Business
San José State University
San José, CA 95192-0219

# TECHNICAL REPORT DOCUMENTATION PAGE

| 1. Report No.<br>20-25 | 2. Government Accession No. | 3. Recipient's Catalog No. |
|---|---|---|
| 4. Title and Subtitle<br>Stability of Fiber-Reinforced Bridge Bearings under Compression and Shear Loads | | 5. Report Date<br>July 2020<br>6. Performing Organization Code |
| 7. Authors<br>Andrea Calabrese, PhD<br>Simone Galano<br>Nghiem Tran | | 8. Performing Organization Report<br>CA-MTI-1929 |
| 9. Performing Organization Name and Address<br>Mineta Transportation Institute<br>College of Business<br>San José State University<br>San José, CA 95192-0219 | | 10. Work Unit No.<br>11. Contract or Grant No.<br>ZSB12017-SJAUX |
| 12. Sponsoring Agency Name and Address<br>State of California SB1 2017/2018<br>Trustees of the California State University<br>Sponsored Programs Administration<br>401 Golden Shore, 5th Floor<br>Long Beach, CA 90802 | | 13. Type of Report and Period Covered<br>Final Report<br>14. Sponsoring Agency Code |
| 15. Supplemental Notes<br>DOI: 10.31979/mti.2020.1929 | | |


**16. Abstract**

Fiber-Reinforced Bearings (FRBs) have proven to be a valuable rubber-based base isolation technology in which flexible fiber reinforcements are used to replace the steel layers commonly adopted for the manufacturing of Laminated Rubber Bearings (LRBs). Thanks to the low weight and cost of FRBs, these devices could prove to be instrumental for the promotion of base isolation applications to houses and residential buildings of developing countries in seismic regions. This report presents the results of a large set of Finite Element Analyses (FEAs) aimed at assessing the performance of FRBs under combined axial and shear loads. The effects of different magnitudes of axial pressure, material properties, and primary and secondary bearing shape factors on the stability of the devices under combined axial and shear loads are discussed in this work. Conclusions of this study underline that the simple design formulae commonly adopted for FRBs underestimate the effect of the axial pressure in limiting the lateral displacement capacity of the bearings. Additional Finite Element Analyses are needed to extend the results of this study to bearings of other shapes, including circular and square isolators.


| 17. Key Words<br>Base isolation, recycled rubber, fiber-reinforced bearings, instability, Finite Element Analyses | 18. Distribution Statement<br>No restrictions. This document is available to the public through The National Technical Information Service, Springfield, VA 22161 | | |
|---|---|---|---|
| 19. Security Classif. (of this report)<br>Unclassified | 20. Security Classif. (of this page)<br>Unclassified | 21. No. of Pages<br>35 | 22. Price |

Form DOT F 1700.7 (8-72)

DOI: 10.31979/mti.2020.1929

Mineta Transportation Institute
College of Business
San José State University
San José, CA 95192-0219

Tel: (408) 924-7560
Fax: (408) 924-7565
Email: mineta-institute@sjsu.edu

transweb.sjsu.edu

071920

# ACKNOWLEDGMENTS

The authors thank Editing Press, for editorial services, as well as MTI staff, including Executive Director Karen Philbrick, PhD; Deputy Executive Director Hilary Nixon, PhD; Graphic Designer Alverina Eka Weinardy; and Executive Administrative Assistant Jill Carter.

# TABLE OF CONTENTS

# LIST OF FIGURES

# LIST OF TABLES

# I. INTRODUCTION

Rubber-based structural devices have been widely adopted in building and bridge engineering.[1] These devices include elastomeric pads, Laminated Rubber Bearings (LRBs), and a large variety of elastomeric isolators that have been manufactured using neoprene and/or natural rubber compounds.[2,3,4] In LRBs for buildings or bridges, steel or fiber reinforcements are widely adopted. In Fiber Reinforced Bearings (FRBs), fiber reinforcements are used instead of the steel plates of conventional laminated devices. FRBs have many advantages over conventional steel reinforced ones:

- FRBs are lighter than LRBs because layers of fibers are adopted instead of heavy steel shims;[2]
- FRBs can be produced with a cost-saving cold vulcanization process;[3]
- FRBs can be cut to the required shape and size from pads of large dimensions, avoiding the vulcanization of an individual device in a mold, which is required for the manufacturing of LRBs;[4]
- When FRBs are adopted in unbounded configurations and sheared in the horizontal direction, the tensile stress at the edges of the bearing is substantially reduced compared to bonded LRBs with similar mechanical characteristics. This is because, if unbonded, FRBs are free to roll off from the supports.[5,6,7]

Due to the advantages of FRBs over conventional LRBs, Kelly[2] investigated the feasibility of adopting these devices as base isolators in developing regions of the world. A substantial research effort has been dedicated to the validation of FRBs' utility for structural control. The research studies on these bearings have included experimental tests in compression[8,9,10] and shear,[11,9] numerical studies of bearings of different shapes and dimensions,[5] and analytical studies for the assessment of the stiffness of the bearing and the stress distribution in the fiber layers when axial loads and lateral deformations are applied.[5]

Kelly and Calabrese studied the effects of the compressibility of the rubber and of the stretching of the reinforcement on the response of an FRB under axial loads.[12] The researchers also addressed the behavior of unbounded stripe-shaped FRBs under lateral loads.[5] Kelly and Calabrese determined that when increasing lateral deformations are applied to FRBs, these devices, after an initial stable deformation, reach a peak in their force deformation response for a displacement corresponding to half of the base of the bearing. This result is only applicable to lightly loaded bearings, as the effect of the axial load on the stability of the bearing is not considered in the design formula presented by the authors. While the study by Kelly and Calabrese[12] considered quasi-static loading conditions, the extension of these results to cyclic deformations was presented in Pauletta et al.[13] The work by Pauletta et al. discusses the feasibility of adopting a bi-linear model of hysteresis to capture the response of FRBs under cyclic shear deformations.

For what concerns the buckling capacity of FRBs, a closed-form solution for isolators with flexible reinforcements was proposed by Tsai and Kelly.[14] The authors determined the stress

distribution in the elastomeric layers under compression, bending and warping, in order to then use these solutions for the definition of the buckling load of stripe-shaped isolators with flexible reinforcements within the framework of the beam theory they developed.[15] The influence of an imposed lateral deformation on the FRBs' axial load-carrying capacity was not discussed in the research by Tsai and Kelly.

Results of Finite Element Analysis (FEAs) aiming at evaluating the stability of FRBs under combined axial and lateral loads are discussed in Osgooei et al.[3] The authors determined the lateral force/displacement response of bounded and unbounded FRBs. They determined that for a bonded FRB, the secant stiffness at peak lateral response is not influenced by an imposed lateral displacement. For unbonded devices, the authors found that the axial load-carrying capacity of a bearing changes with the applied lateral deformation. The response of unbonded FRBs was attributed to the variation of the resisting area of the device during the roll-off deformation. Results of the study discussed in Osgooei et al. are based on the analysis of two finite element models having the same overall dimensions and the same material properties. Nevertheless, the results discussed in that work are only applicable to large and stable devices. As far as the authors' knowledge, none of the research works available in the literature include considerations of the influence of the geometry of the bearing, the effect of different primary and secondary shape factors, or material properties such as the shear modulus and the compressibility of the elastomer on the stability of FRBs under combined axial and shear loads. Results of experimental tests considering the simultaneous application of axial and lateral loads are discussed in Toopchi-Nezhad et al.,[16] where FRBs tested under cyclic loads met base isolation requirements for both shear stiffness and energy dissipation. It is worth mentioning that the experimental tests performed by Toopchi-Nezhad et al. aimed at assessing the response of stable devices with large shape factors (i.e., devices with a large ratio of base to height). The tested bearings proved to be stable under a maximum axial pressure of 2.4 MPa and large imposed displacements.

Other stable devices have been tested by de Raaf et al.[18] The authors discuss the results of tests performed on four FRBs with the aim of determining the effects of the amplitude of imposed lateral displacements, history of loading, and vertical pressure on the response of unbonded FRBs. While that study offers insight into the response of FRBs under combined axial and lateral loads, the extent of the experimental tests presented by de Raaf et al. is not sufficient to draw general conclusions or to extrapolate, from these results, claims about the response of bearings of different material properties or primary and secondary shape factors.

With these considerations in mind, the research here presented aims to shed some light on the behavior of unbonded FRBs loaded in compression and shear. Given this scope, FEAs have been performed to determine the peak lateral displacement and axial load-carrying capacity of unbonded FRBs. The influence of different axial loading conditions, material properties, and primary and secondary shape factors of the bearings on their vertical and lateral response are herein discussed. Numerical models of FRBs have been analyzed using advanced tools for FEAs. Results of this work are based on analyses considering all forms of nonlinearities including material, geometric, and contact nonlinearities.

# II. STABILITY OF UNBONDED FRBS, ANALYTICAL MODELS

## LATERAL DISPLACEMENT CAPACITY OF UNBONDED FRBS

Easy-to-use design formulae for the determination of the peak and ultimate lateral displacement capacity of FRBs are given in Kelly and Calabrese.[5] The authors verified that when unbonded FRBs are loaded in shear, they detach from the upper and lower horizontal surfaces. The resisting area of the bearing reduces and the isolators reach a peak resisting capacity, defined by a zero-tangent stiffness, for a horizontal displacement corresponding to half of the base of the bearing. In the study by Kelly and Calabrese, this level of deformation is defined as peak displacement. Past the peak resisting capacity of the bearing, an FRB can be sheared up to the full rotation of the vertical surfaces of the device, corresponding to a complete roll-over. This level of deformation is defined as ultimate displacement. Because the friction between the rubber layers and the horizontal steel subgrades is very large, deforming a bearing past the ultimate displacement would result in damage to the device.

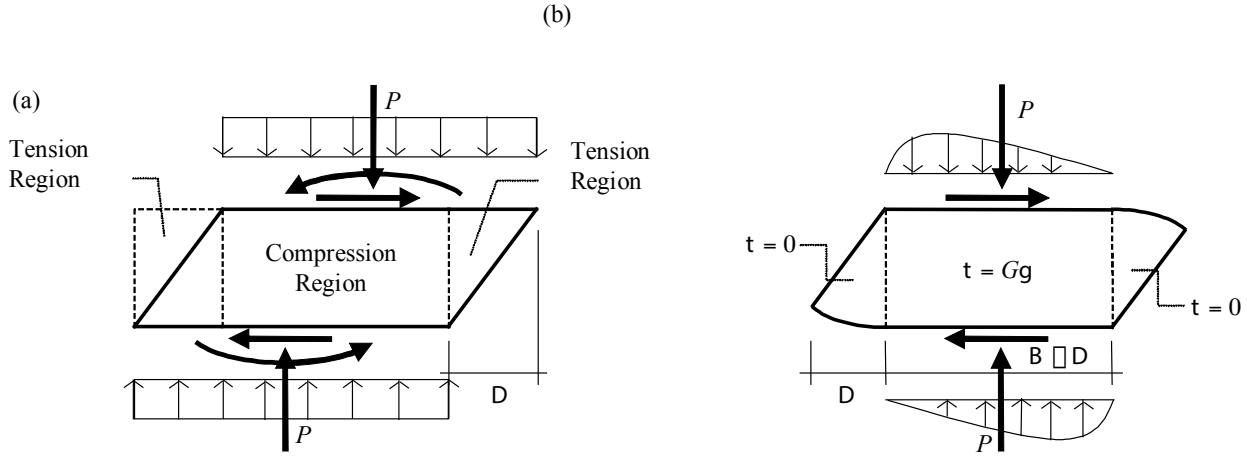


**Figure 1. Schematic of an Unbounded Bearing Loaded in Compression and Shear (from Kelly and Calabrese[5])**

Figure 1 shows the fundamental hypothesis at the base of the analysis: the areas that rolled off the supports are stress-free, while the area between the contact surfaces is assumed to resist the imposed deformation while developing a constant shear stress. The lateral resisting force per unit length of a strip-type bearing can be written as $F = G\gamma \cdot (B - \Delta) = G \cdot (B - \Delta) \cdot \Delta / t.$ From this equation, it is clear that an FRB remains stable (i.e., positive tangent to force/ displacement curve) up to the zero slope point, where $dF / d\Delta = G / t \cdot (B - 2\Delta) = 0$, corresponding to a displacement $\Delta$ equal to half of the base *B* of the device. As a result, once the design displacement is defined depending on the hazard at the site, the damping of the isolation layer, and the design period of vibration, the condition for the stability of an FRB can be met if $B \geq 2\Delta$. The ultimate displacement of an FRB is determined assuming that (i) the rubber is incompressible, (ii) the fiber reinforcements do not contribute to the bending stiffness of the bearing, and (iii) the lateral areas of an unbonded FRB are stress-free. Based on these assumptions, Calabrese and Kelly, determined that the ultimate displacement of an FRB is equal to twice the total thickness of the elastomer. This result defines the maximum displacement capacity of a base isolation layer on FRBs. While these

formulas are easy to use and allow for an immediate determination of the size of the bearing, the theoretical solution proposed by Kelly and Calabrese does not take into account the thickness of the individual fiber layer, the compressibility of the rubber and the mechanical properties of the device in shear.

## THE BUCKLING AND POST-BUCKLING ANALYSIS OF LONG STRIP BEARINGS

Kelly and Marsico[19] analyzed the buckling and post-buckling response of long strip bearings. The authors studied bearings of strip shape because (i) these are easy to model, and (ii) these devices are suited for applications to bridge engineering and as base isolators of masonry buildings.

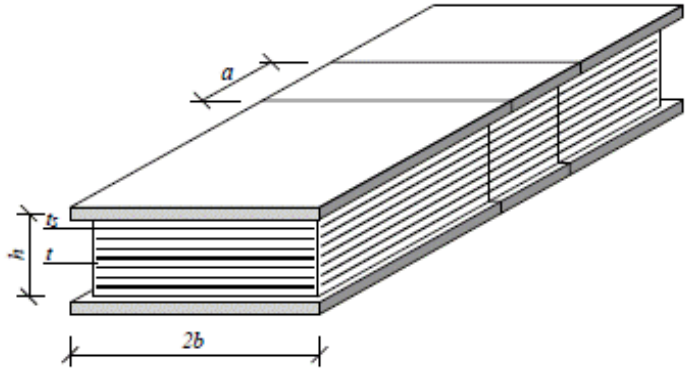


**Figure 2. An Infinite Strip Pad of Width 2b (adapted from Kelly and Marsico[19])**

The model considered for the analysis is shown in Figure 2, where 2*b* is the base of the bearing, *t* is the thickness of the rubber layer, *n* is the number of layers, and $t_s$ is the thickness of the individual fiber reinforcement. The analysis of the pad is based on the following hypotheses:

- The fiber reinforcement has no flexural rigidity;
- The vertical load is carried by the overlap area;
- The roll-off portion of the bearing is stress-free.

Under increasing lateral deformations, the bearings start to roll off from the supports, the overlap area reduces (i.e., the vertical stiffness of the bearing reduces), and the buckling load reduces, while the vertical displacement increases.[4] This geometric nonlinearity was studied by Tsai and Kelly.[14] The authors determined that the vertical displacement due to geometric nonlinearity, $\mathrm{d}_v^G$, arising from a horizontal deformation is equal to:

$$\delta_v^G = \frac{\pi G A_S}{4 P_{crit}} \left( \frac{\pi p - \sin \pi p}{1 - \cos \pi p} \right) \frac{\delta_h^2}{h} \qquad (1)$$

where $p = P / P_{crit}$ is the ratio between the applied load $P$ and the critical load $P_{crit}$, obtained as:

$$P_{crit} = \left(\frac{\pi}{h}\right)(EI_s GA_s)^{1/2}. \quad (2)$$

Substituting Equation 1 into Equation 2 yields:

$$\delta_v^G = \frac{1}{4}\left(\frac{GA_s}{EI_s}\right)^{1/2}\left(\frac{\pi p - \sin \pi p}{1-\cos \pi p}\right)\delta_h^2 \quad (3)$$

The buckling load in the undeflected configuration can be obtained by substituting the expressions for the effective shear stiffness per unit length ($GA_s$) and the effective bending stiffness per unit length ($EI_s$) in Equation 2 to obtain:

$$P_{crit} = \frac{4\pi G b^3}{\sqrt{15} n t^2} \quad (4)$$

The vertical displacement corresponding to the vertical load $P_{crit}$ in the undeflected configuration can be obtained by dividing the critical vertical load over the vertical stiffness of the bearing, obtaining:

$$\delta_v^C = \frac{P_{crit}}{K_v} = \frac{\pi}{2\sqrt{15}} t \quad (5)$$

It is worth mentioning that this displacement is only a function of the thickness of the rubber layer *t*. This means that when the overlap area is reduced by the applied lateral displacement, the vertical displacement under the critical load remains the same. The critical load for an overlap area of $(2b-\delta_h)$ was determined to be:

$$P_{crit}(\delta_h) = \frac{4\pi G\left(2b-\delta_h\right)^3}{\sqrt{15} n t^2} \quad (6)$$

The ratio of the critical load under an imposed horizontal displacement over the critical load of the undeformed bearing (i.e., Equation 2 over Equation 6) gives:

$$\frac{P_{crit}(\delta_h)}{P_{crit}} = p(\delta_h) = \left(1-\frac{\delta_h}{2b}\right)^3 \quad (7)$$

When the vertical load exceeds the critical value, it is necessary to modify the vertical displacement expression to consider the geometric nonlinearity induced by an applied lateral deformation; by substituting Equation 5 in Equation 3, the following expression is obtained

$$\delta_v^G = \frac{1}{4}\left(\frac{15}{2S^2 b}\right)^{1/2}\left(\frac{\pi p - \sin \pi p}{1-\cos \pi p}\right)\delta_h^2 \quad (8)$$

It is therefore possible to use this relation to calculate the horizontal displacement due to an increasing vertical load:

$$\frac{\delta_h}{2b} = \frac{\sqrt{\frac{2}{15}}(x-1)^{1/2}}{1+\sqrt{\frac{2}{15}}(x-1)^{1/2}} \tag{9}$$

where:

$$x = \frac{\delta_v}{\pi t / 2\sqrt{15}} \tag{10}$$

Substituting Equation 9 in Equation 8, the variation of the vertical load can be written as:

$$p(\delta_h) = \left(1+\sqrt{\frac{2}{15}}(x-1)^{1/2}\right)^{-3} \tag{11}$$

Developing this function in a McLaurin series and truncating to the second order, an approximation of the post-buckling load is obtained as:

$$p(\delta_h) = 1-3\sqrt{\frac{2}{15}}(x-1)^{1/2} \tag{12}$$

These results are plotted in Figure 3.

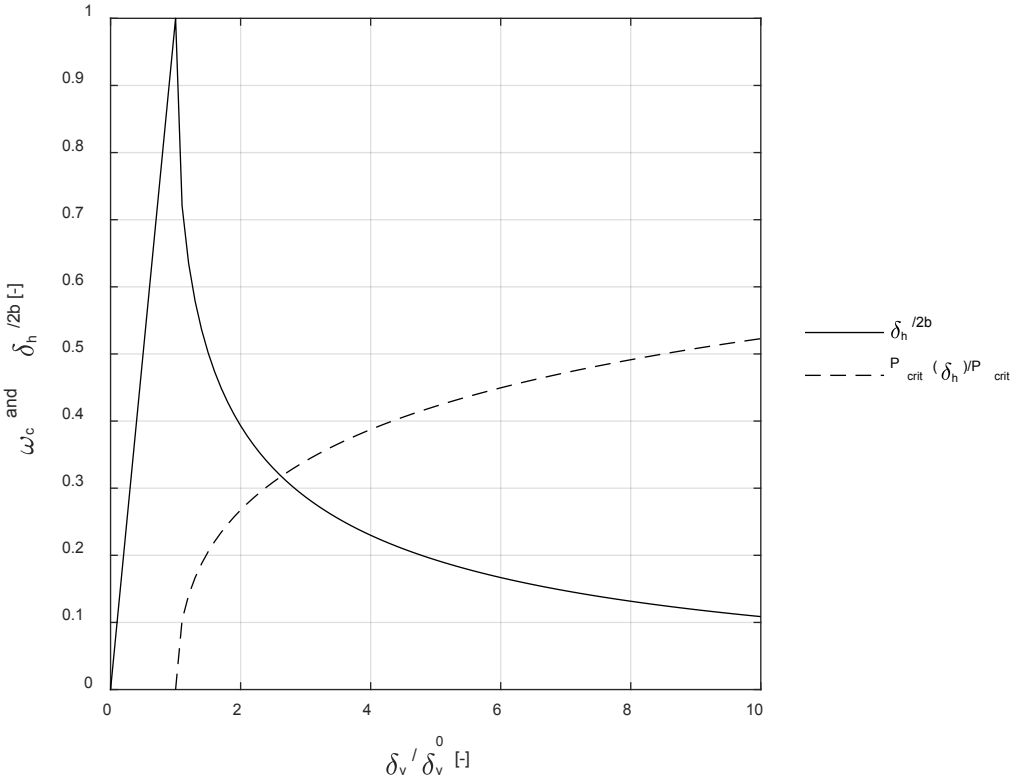


**Figure 3. Trend of the Normalized Critical Load as a Function of the Normalized Vertical Displacement (from Kelly and Marsico[19])**

## VERTICAL DISPLACEMENT OF THE TOP OF THE BEARING FOR AN INFINITE STRIP

It is possible to compute the total vertical displacement at the top of the bearing, superimposing the contributions deriving from the shortening of the bearing due to the vertical load ($d_v^0$) and those due to the geometric nonlinearity induced by an applied lateral displacement ($d_v^G$):[4]

$$\delta_v^t = \delta_v^0 + \delta_v^G \tag{13}$$

When the applied horizontal displacement is zero, the vertical displacement only depends on the applied vertical load, and it is given by the following expressions:

$$\delta_v^t(P) = \frac{P t_r t^2}{8Gb^3}$$
$$\delta_v^t(P_{crit}) = \frac{\pi t}{2\sqrt{15}} \tag{14}$$

When a lateral deformation is applied to the bearing, the vertical displacement can be written as:

$$\delta_v^t = \frac{\pi}{16}\frac{t}{\left(b-\delta_h/2\right)^2}\sqrt{15}\delta_h^2 + \frac{\pi t}{2\sqrt{15}} \tag{15}$$

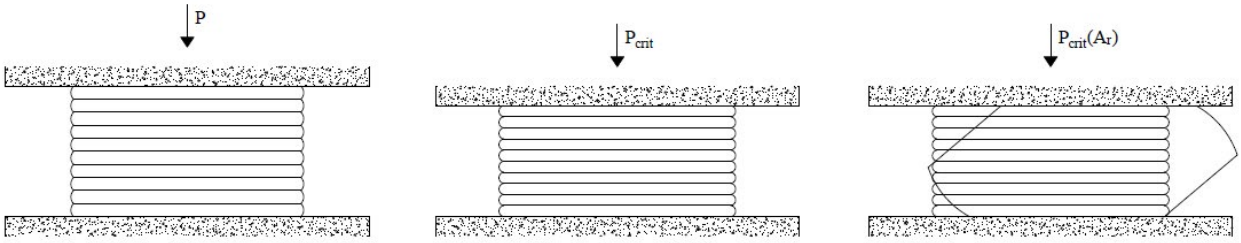


**Figure 4. Deformed Shape of an FRB Under Critical Load in the Vertical Direction, Applied on the Reduced Area**

# III. FINITE ELEMENT ANALYSIS OF UNBOUNDED BEARINGS

The Finite Element Analyses of unbonded rubber bearings with flexible reinforcements under combined axial and lateral load is challenging because it requires advanced numerical tools to capture highly nonlinear phenomena such as those occurring in an FRB under large lateral displacements and loads. The nonlinearities include sliding of the bearing at the contact surfaces, variation of the boundary conditions, large strain of the elastomer and its near incompressibility, and self-contact of the edges of the bearing, which can be deformed enough to fold over themselves. It is worth mentioning that conventional FEAs are not suited to capture the near incompressibility of the rubber, thus producing weak results or ill-conditioning issues, where volumetric mesh-locking can easily occur.[22] Some combined methods have been recently developed for the analysis of nearly incompressible and incompressible materials:[19] they are based on the variational principles of Hellinger-Reissner and Hu-Washizu, which consider both stresses and strains as unknowns. The analyses discussed in this report are based on the popular Herrmann[21] mixed method, which is a special case of the more general Hellinger-Reissner variational principle. The software used for the analyses discussed in this report (i.e., Marc from MSC software[22]) has been purposefully built to simulate the response of elastomeric materials, and it includes many constitutive laws for elastomers, such as the Mooney–Rivlin and the Boyce–Arruda material models. Within the software, a variety of element types can be used to accurately simulate the response of components undergoing large strains. The FEAs discussed in this study are based on two-dimensional models where a plane strain is assumed to match the response of a rectangular or strip-type isolation bearing loaded in shear.

## MATERIAL AND CONTACT MODELS USED FOR THE ANALYSES

For the FEA models discussed in this work, the reinforcing fiber elements are modeled using a rebar, i.e., an element working in tension/compression made of a material with linear elastic isotropic behavior. A rebar is characterized by its thickness, $t_f$, and Young's modulus, $E_f$. A single-parameter material of Mooney–Rivlin type (that is, a Neo-Hookean material) has been adopted to simulate the elastomer. For this material model, the strain energy function is based on the bulk modulus, $K$, and the shear modulus, $G$. For incompressible solids of Mooney–Rivlin type, the strain energy density function, $W$, is obtained by linearly combining the first ($\bar{I}_1$) and the second ($\bar{I}_2$) invariant of the deviatoric component of the left Cauchy–Green deformation tensor:

$$W = C_1(\bar{I}_1 - 3) + C_2(\bar{I}_2 - 3) \tag{16}$$

$$\bar{I}_1 = J^{-2/3} I_1 \quad I_1 = \lambda_1^2 + \lambda_2^2 + \lambda_3^2 \quad J = \det(F) \tag{17}$$

$$\bar{I}_2 = J^{-4/3} I_2 \quad I_2 = \lambda_1^2\lambda_2^2 + \lambda_2^2\lambda_3^2 + \lambda_1^2\lambda_3^2 \tag{18}$$

In Eqs. 16 to 18, $F$ is the deformation gradient, and $J$ is equal to 1 for an incompressible material, while $C_1$ and $C_2$ are material constants to be determined from experimental tests on the elastomer. In the special case of a Mooney–Rivlin incompressible material under uniaxial tension, the stress/strain equation becomes the following:

$$\sigma = 2\left[(1+\varepsilon)-(1+\varepsilon)^{-2}\right]\cdot\left[C_1 + C_2(1+\varepsilon)^{-1}\right] \quad (19)$$

The initial shear modulus is $G = 2(C_1 + C_2)$. For an incompressible material, the initial tensile modulus $E$ can be obtained as $6(C_1 + C_2)$. The FEAs discussed in this work use four-node quadrilateral and isoparametric elements (that is, element type 80 in Marc) to model the elastomer. These elements use bilinear interpolation functions, and the strain deformation remains constant over each element. Because of this reason, a fine mesh is needed when performing FEAs of rubber components using element type 80 in Marc. Using this element, a four-point Gaussian integration can be adopted to determine the stiffness of the element. A Gaussian integration can be assumed for small strains as well as large strains. In the analyses, rigid lines and Coulomb friction are used to simulate the top and bottom support surfaces. A contact setting embedded in MSC.Marc 2005[21] is used for the analyses, which is able to detect a deformable body to deformable body contact, or a deformable body to rigid body contact, as happens in an FRB under the simultaneous effects of compression and large lateral displacement demands.

The geometry and discretization of a typical Finite Element model tested for the analyses are shown in Figure 5. The mesh of the model is denser at the top and bottom boundaries, where the largest distortion of the quadrilateral elements occurs during the analysis. The size of the mesh was defined by performing a sensitivity study for each of the tested models.

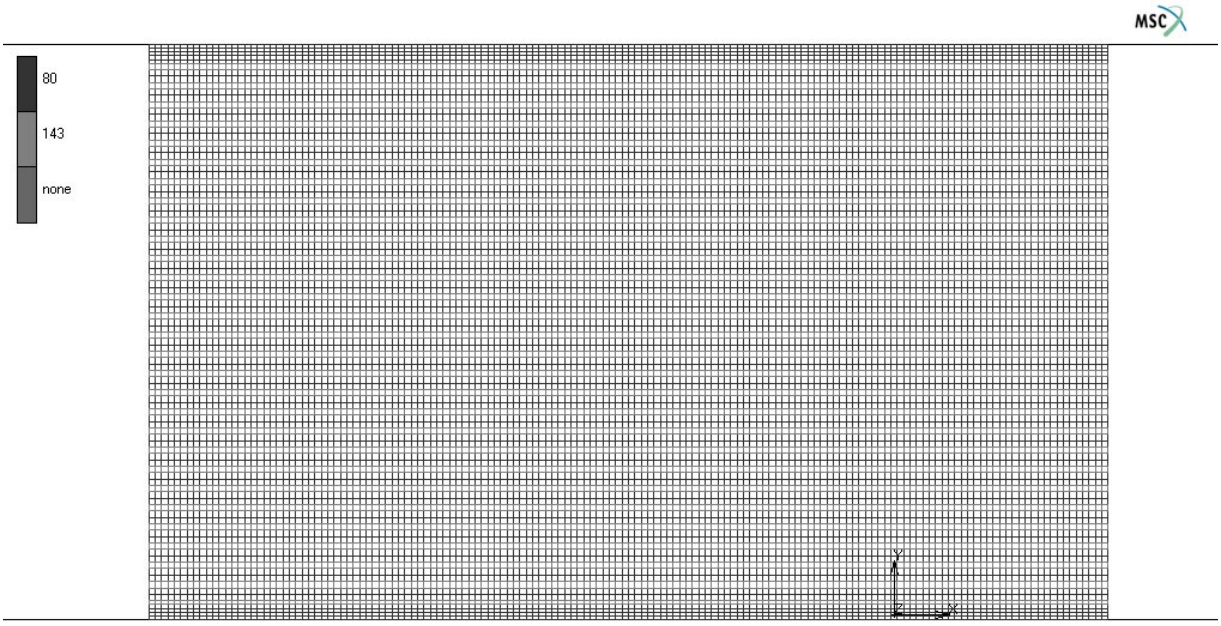


**Figure 5. Typical Geometry and Discretization of a Fiber-Reinforced Bearing for FEAs**

## DESCRIPTION OF THE ANALYSIS SET

A large variety (c.a., 4320 models) of two-dimensional FEMs of FRBs has been tested for this study. The plain strain assumption was used for the analyses, with the out-of-plane dimension for all the bearings assumed to be equal to 750 mm. For the base of the bearings, $B$, the increasing values of 250, 300, 350, 400, 450, and 500 mm were considered. Two-dimensional analyses were preferred to three-dimensional ones, because the former allow a clear understanding of the out of plane response of strip-type bearings without the computational effort required for the analysis of three-dimensional isolators. For the thickness of the rubber layers, $t_r$, the values of 5, 10, and 15 mm were considered. These assumptions correspond to values of the primary shape factor, $S_1$ (defined for the single layer of elastomer as the ratio of the total loaded area to the load-free area = $B$ / $2t_r$) in the range 8.5 to 50. The height of all the bearings, $H$, was set to 180 mm. The secondary shape factor $S_2$ was defined as $B$ / $H$. This assumption corresponds to secondary shape factors $S_2$ in the range of 1.38 to 2.78. Elastomers with different shear moduli ($G$ = 0.5; 0.7; 0.9; 1.1 MPa) and different bulk moduli ($K$ = 1400; 1600; 1800; 2000 MPa) were considered. A summary of all the tested models for this parametric study is given in Table 1, with a sketch of the FRB models given in Figure 6.

**Table 1. Summary of the Models Considered for FEAs**

| $B$ | $H$ | $t_r$ | Shear Modulus, $G$ | Bulk Modulus, $K$ | $s_v$ |
|---|---|---|---|---|---|
| [mm] | [mm] | [mm] | [MPa] | [MPa] | [MPa] |
| 250 | 180 | 5 | 0.5 | 1400 | 1.5 to 8.5 |
| 300 | | 10 | 0.7 | 1600 | |
| 350 | | 15 | 0.9 | 1800 | with |
| 400 | | | 1.1 | 2000 | increments |
| 450 | | | | | of 0.5 MPa |
| 500 | | | | | |

During the FEAs, the axial load was applied first and held constant; then, a displacement-controlled analysis was performed with increasing displacements up to the complete roll-over of the bearings.

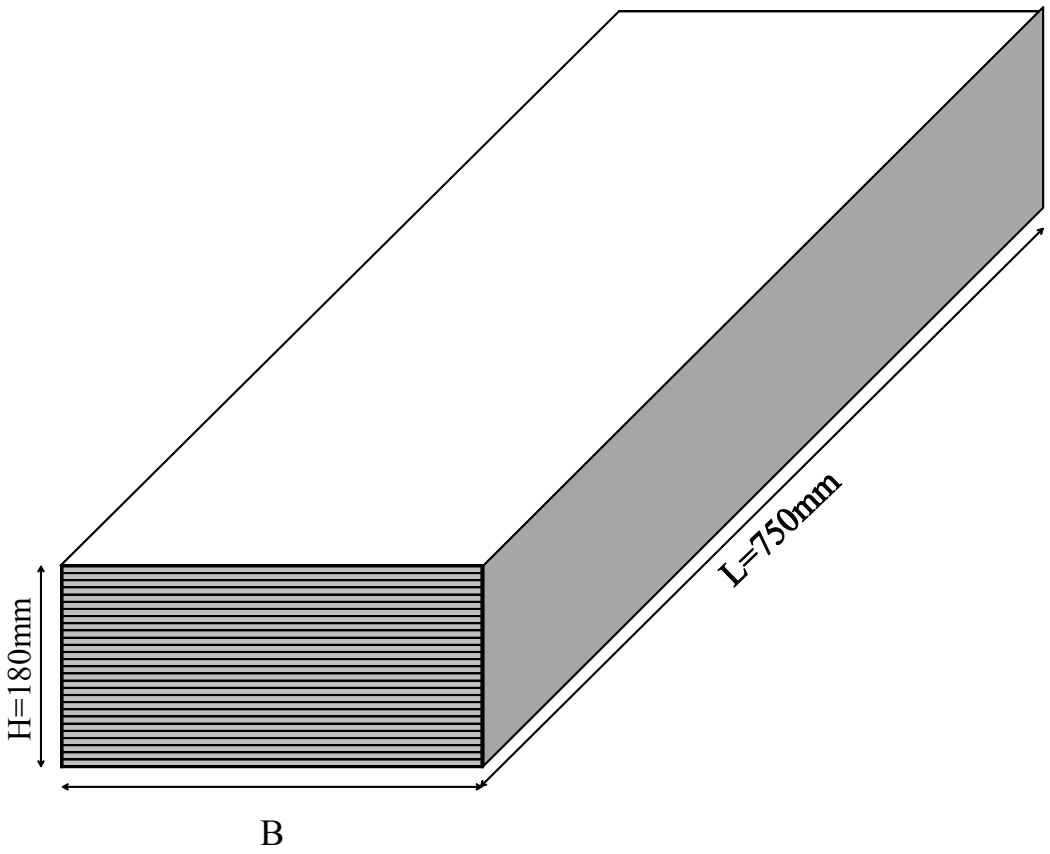


**Figure 6. Geometry of the Strip-Type Isolators Tested for this Study**

## RESULTS OF THE ANALYSES

The typical response of an FRB under combined axial and lateral load is show in Figure 7 through Figure 12. As already discussed in other works,[12] when a bearing with a flexible reinforcement is deformed in shear, as FRBs detach from the lower and the upper surfaces, no tensile stresses are generated at the edges of the bearing. Compared to the application of the axial load, and zero horizontal displacement show in Figure 7, Figure 8, at peak horizontal load, the axial stress in the layers of reinforcement substantially increases (see Figure 15) because of the reduction of the effective area. This effect is less pronounced for bearings with a large base, while for small bearings, an increase of tensile stress up to 200% can be expected in the fiber reinforcements.

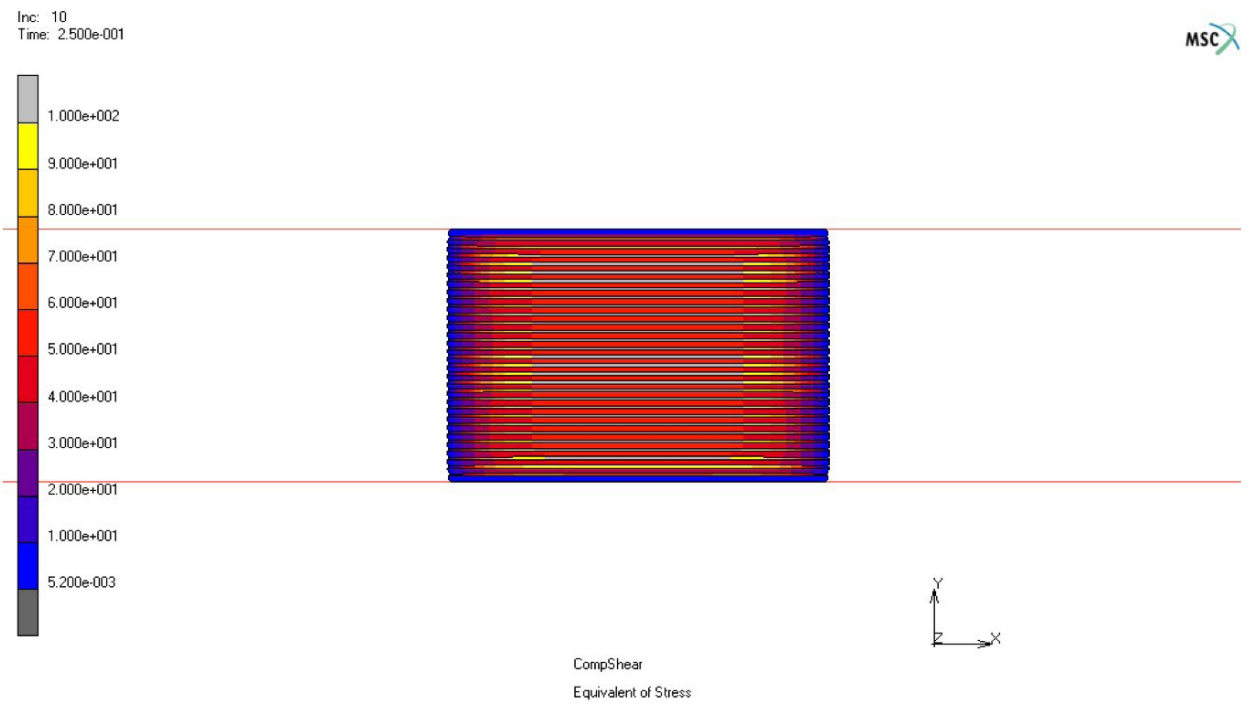


**Figure 7. Von Mises Stress Contours at Peak Vertical Force in a Bearing of Base B = 250 mm**

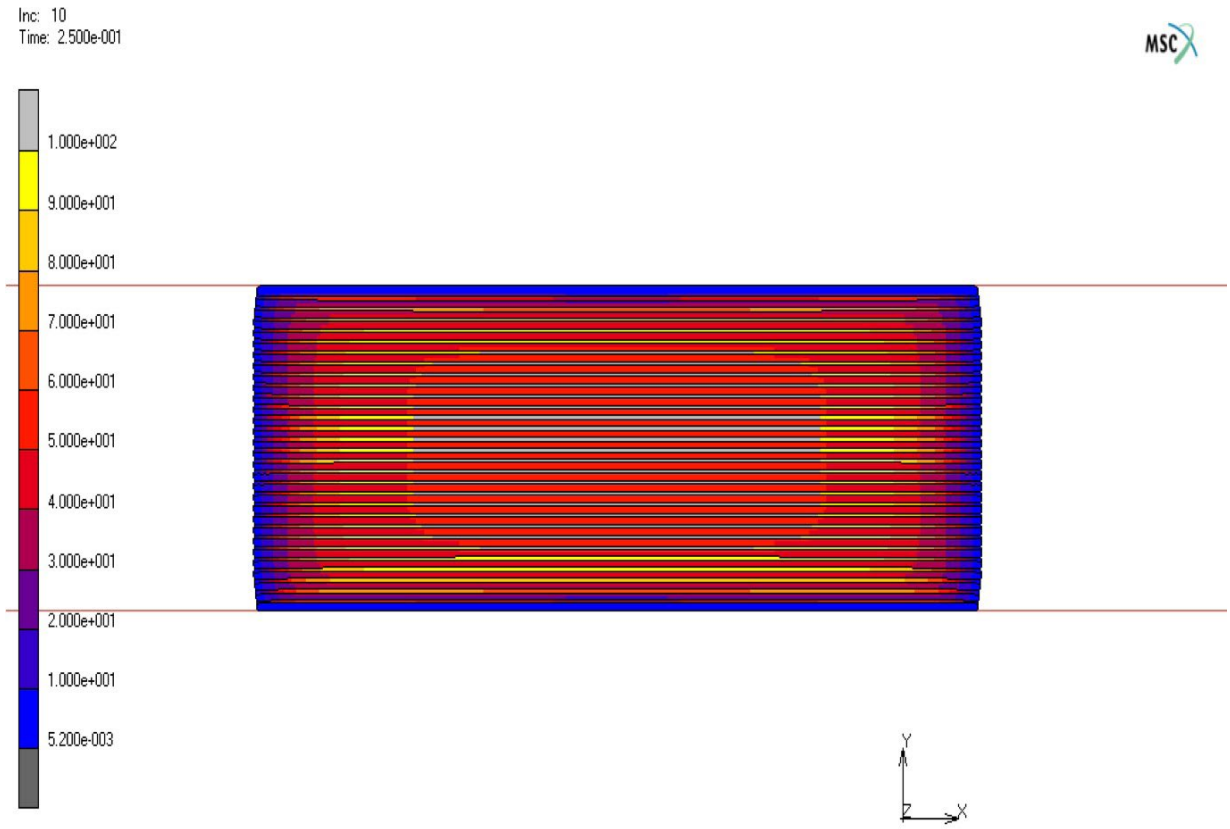


**Figure 8. Von Mises Stress Contours at Peak Vertical Force in a Bearing of Base B = 500 mm**

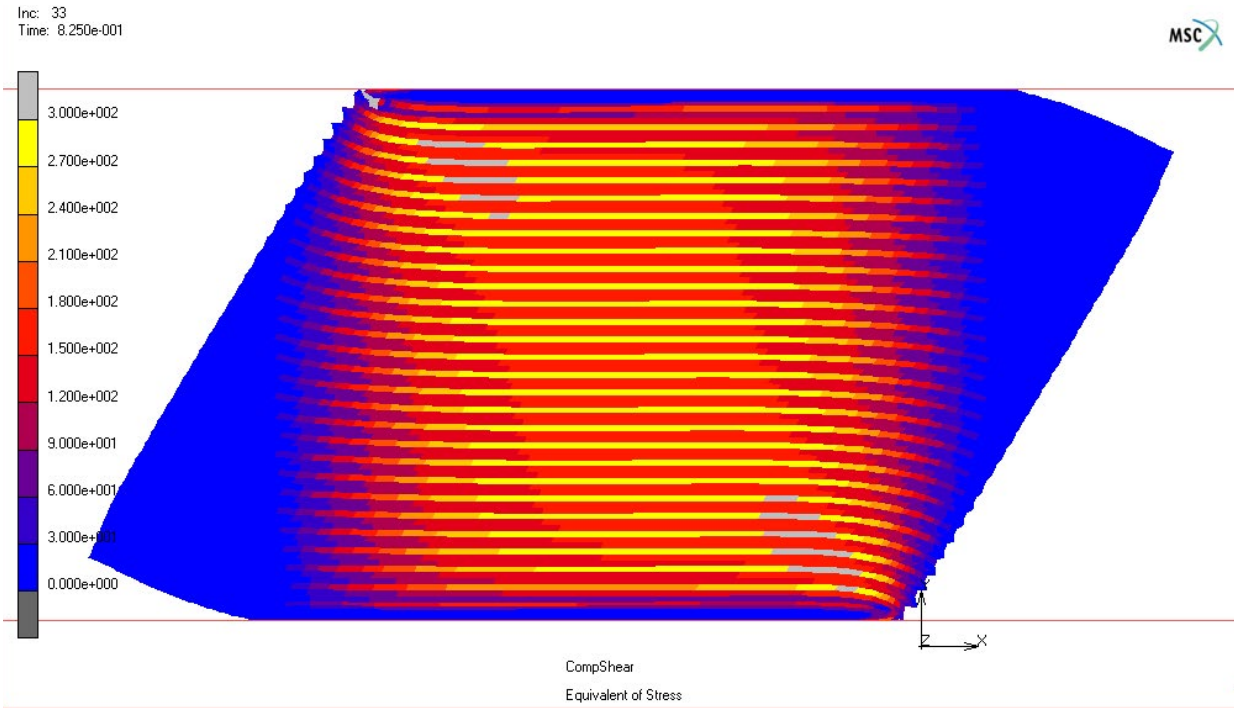


**Figure 9. Stress Contours under Peak Horizontal Loading in a Device with Base B = 250 mm**

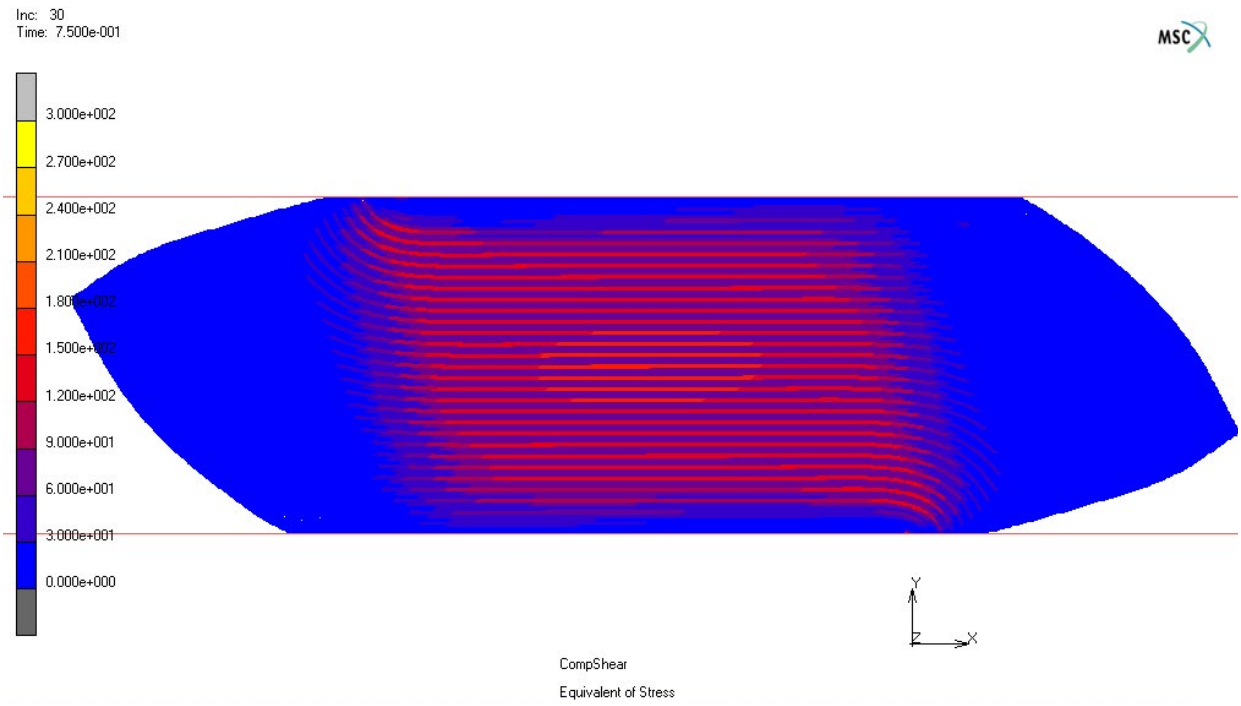


**Figure 10. Stress Contours under Peak Vertical Loading in a Device with Base B = 500 mm**

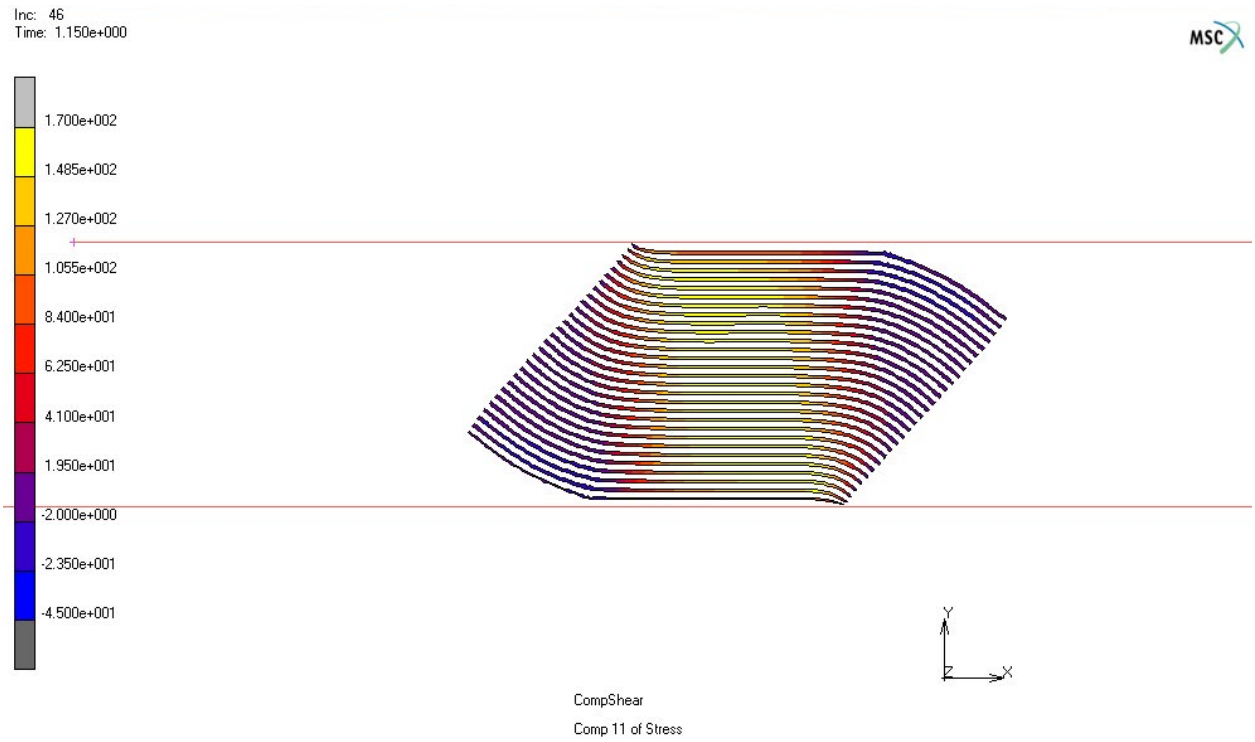


**Figure 11. Tension Contours in the Fibers at the Peak Shear (B = 250 mm)**

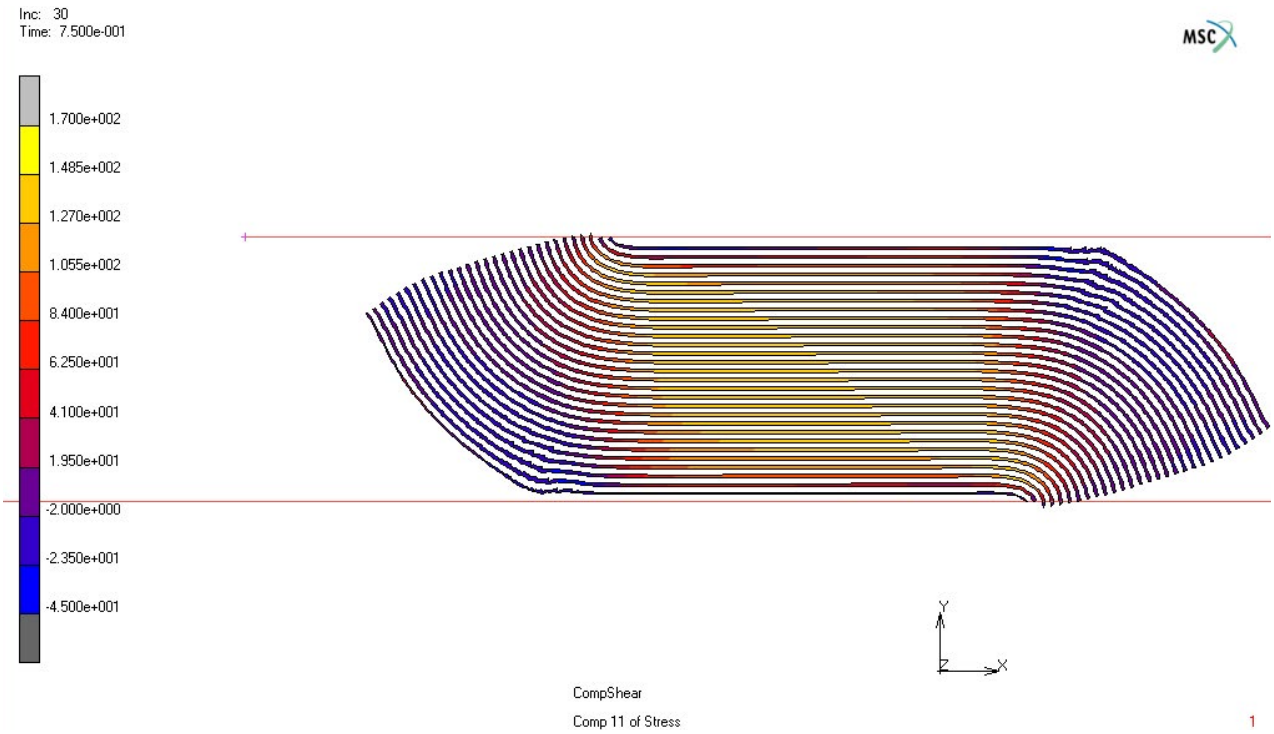


**Figure 12. Tension Contours in the Fibers at the Peak Shear (B = 500 mm)**

It is worth pointing out that during the analyses, some of the tested models failed to meet the convergence criteria under large imposed deformations corresponding to the ultimate shear strain. A solution to the convergence issues of rubber models under large deformations is found in the Global Adaptive Remeshing (GAR) feature of MARC. When this option is

selected, the solver automatically generates a new mesh if certain criteria of distortion, strain change, and/or penetration are met. While the GAR option is very powerful and can be used to simulate the behavior of elastomeric elements where large deformations occur, the feature does not include the remeshing of the layers of reinforcements. For this reason, the GAR option was not used for the analyses, and different geometries of the mesh and densities were tested to obtain satisfactory results for each of the tested models, independently of the level of deformation.

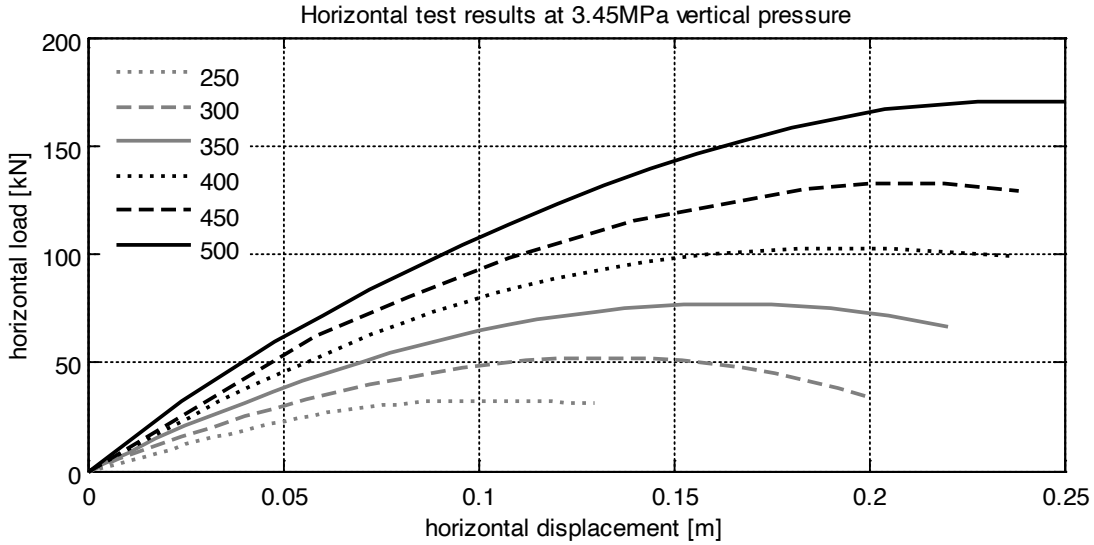


**Figure 13. Force vs. Displacement Curves for Different Isolator Widths**

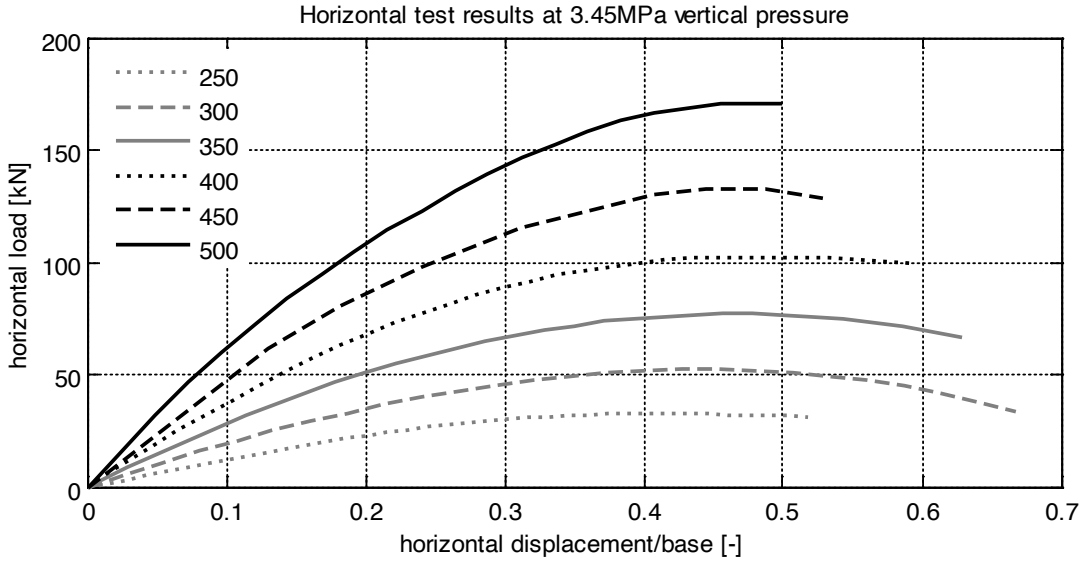


**Figure 14. Force vs. Displacement/Base Ratio for Different Bearing Widths**

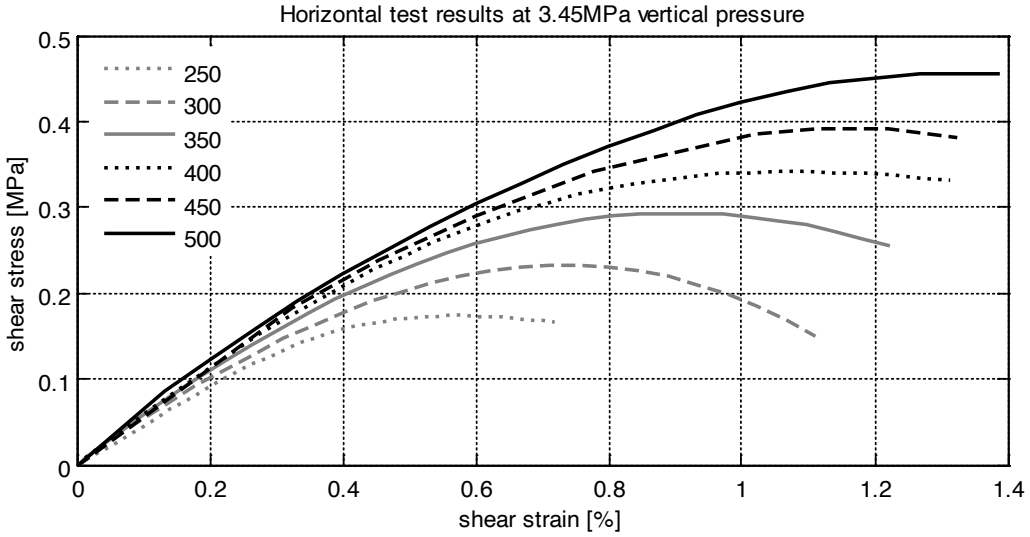


**Figure 15. Stress/Strain Curves in Shear Direction for Different Device Bases**

**Table 2. Ultimate Performance of the Isolators of SET #1 Under Horizontal Load**

| $B$ | $S$ | $F_{h,u}$ | $\tau_u$ | $\Delta_u$ | $\Delta_u / B$ | $\gamma_u$ |
|---|---|---|---|---|---|---|
| [mm] | [-] | [kN] | [MPa] | [mm] | [-] | [%] |
| 500 | 43.48 | 170.5 | 0.45 | 204 | 0.4 | 1.1 |
| 450 | 39.13 | 139.9 | 0.41 | 195 | 0.4 | 1.1 |
| 400 | 34.78 | 104.1 | 0.35 | 190 | 0.5 | 1.1 |
| 350 | 26.09 | 77.17 | 0.29 | 167 | 0.5 | 0.9 |
| 300 | 21.74 | 52.13 | 0.23 | 136 | 0.5 | 0.8 |
| 250 | 43.48 | 32.92 | 0.18 | 104 | 0.4 | 0.6 |

Figure 16 and Figure 17 show the effect of the axial load and of the secondary aspect ratio, $S_2$, on the horizontal response of the devices: an increase of axial pressure clearly determines a reduction of the maximum shear capacity of the bearings. This effect is nonlinear with the applied load, being more pronounced for large compression loads and for bearings with small secondary aspect ratios. The peak lateral load-carrying capacity and the corresponding level of deformation are plotted in Figure 18 and Figure 19 for a bearing of base $B$ = 300 mm, in Figure 24 and Figure 25 for a bearing of base $B$ = 350 mm, and in Figure 30 and Figure 31 for a bearing of base $B$ = 400 mm, under different levels of axial load. As is clear from Figure 18, Figure 24, and Figure 30, the peak shear strain is independent of the shape factor $S$ of the bearings for values of axial pressure in the range 3.5–4.0 MPa, as well as for values of shape factors larger than 30. For $S$ < 30, the effect of the shape factor on the peak shear response of the bearing changes with the vertical pressure, $\sigma_v$: for $\sigma_v < 3.5$ MPa, the deformation capacity increases for $S$ less than 10 and decreases for higher values of $S$; for $\sigma_v > 3.5$ MPa, the maximum deformation capacity decreases when the shape factor is less than 10 and increases for higher values. Regarding the force response of the bearings, it is worth mentioning that the peak shear capacity of the bearings (Figure 19, Figure 25, Figure 31) is not affected by the shape

factor when *S* is larger than 30, but it increases for *S* < 30. The influence of the shear modulus of the rubber, *G*, on the shear strain and stress capacity of the bearings with a base *B* of 300 mm, 350 mm, and 400 mm are plotted in Figure 20 and Figure 21, Figure 26 and Figure 27, and Figure 32 and Figure 33, respectively. The peak shear strain (Figure 20, Figure 26, Figure 32) increases when the shear modulus increases. For values of axial pressure of 6.0 MPa, the increase in shear strain is almost linear with the shear modulus. For smaller values of axial loads, the peak shear strain increases with the axial load, but the response is concave down. For large values of axial load, increasing the shear modulus of the rubber substantially increases the shear load capacity of the bearings. Figure 21, Figure 27, and Figure 33 show that the peak shear stress capacity of an FRB always increases with increased shear modulus, independently of the axial pressure. The influence of the bulk modulus of the rubber on the horizontal response of an FRB is show in Figure 22 and Figure 23 for *B* = 300 mm, Figure 28 and Figure 29 for *B* = 350 mm, and Figure 34 and Figure 35 for *B* = 400 mm. The plots indicate that lateral response of an FRB is not influenced by the bulk modulus of the rubber, with the bulk modulus only slightly changing the peak shear strain of an FRB while having no influence on the shear stress capacity of these devices.

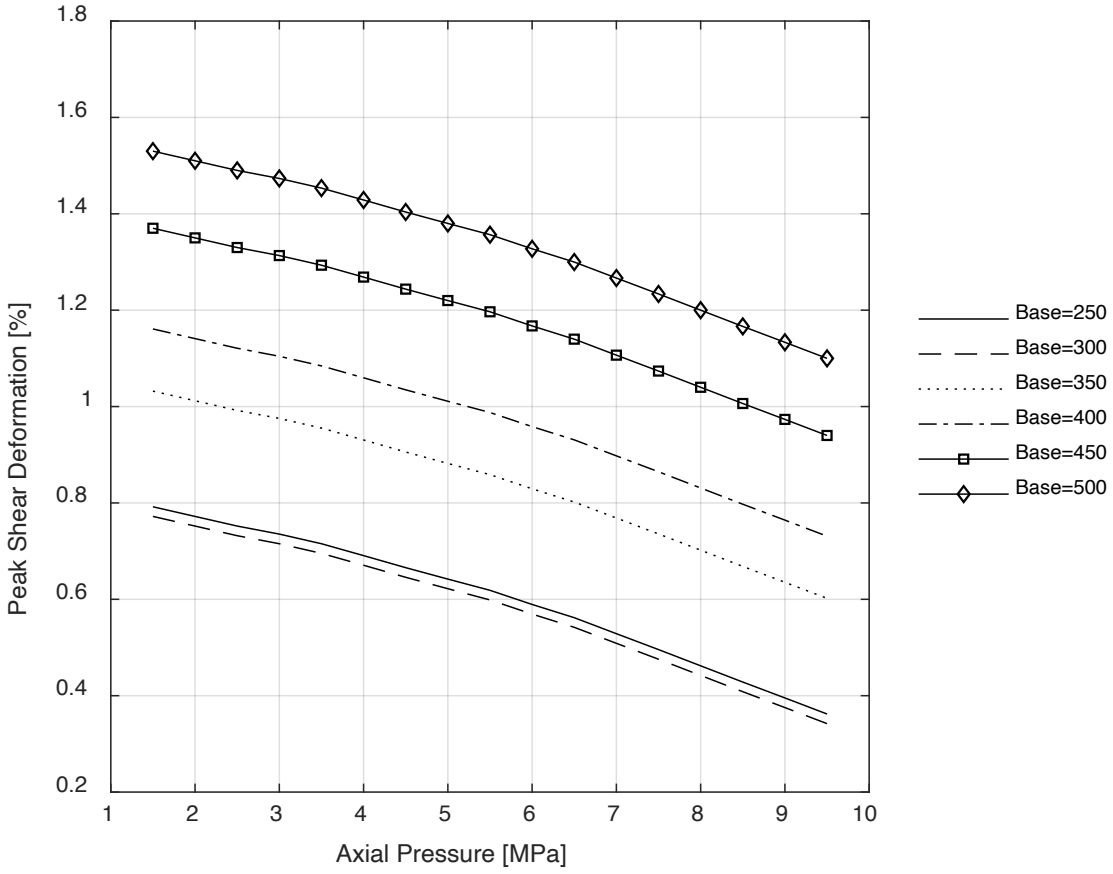


**Figure 16. Peak Shear Strain vs. Axial Pressure**

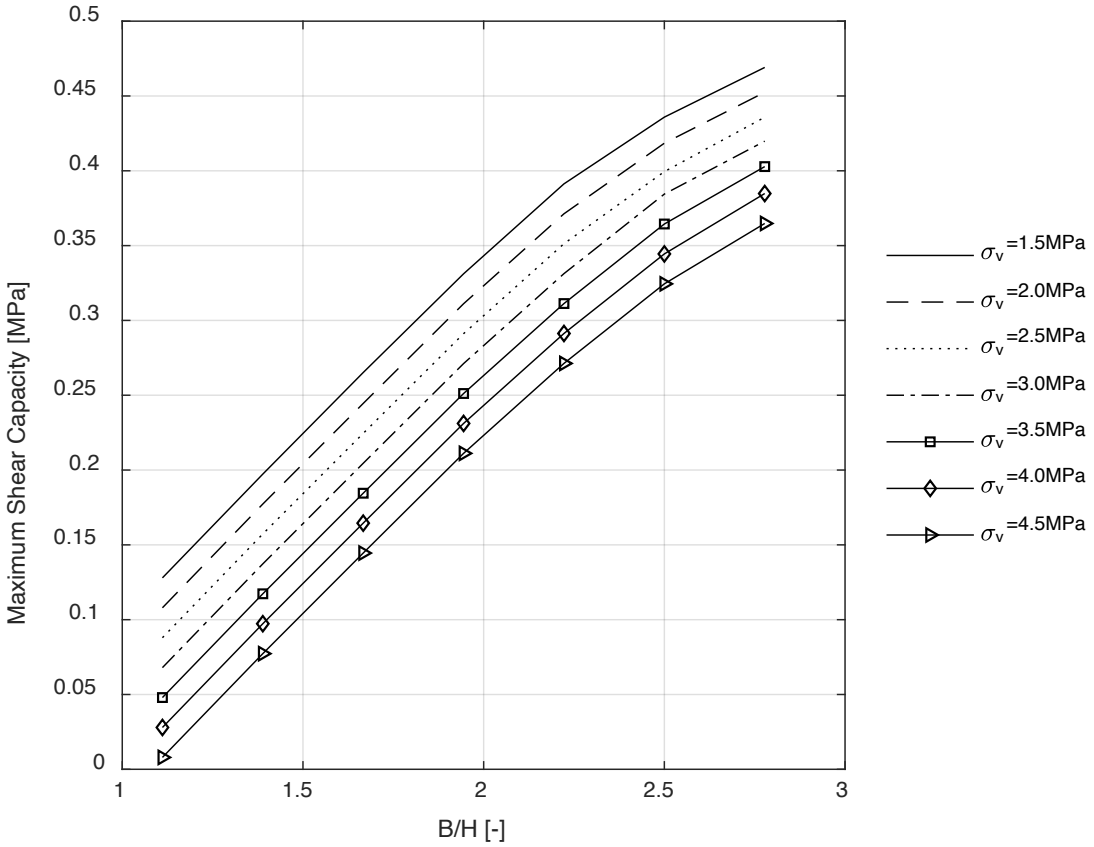


**Figure 17. Maximum Shear Stress vs. Aspect Ratio**

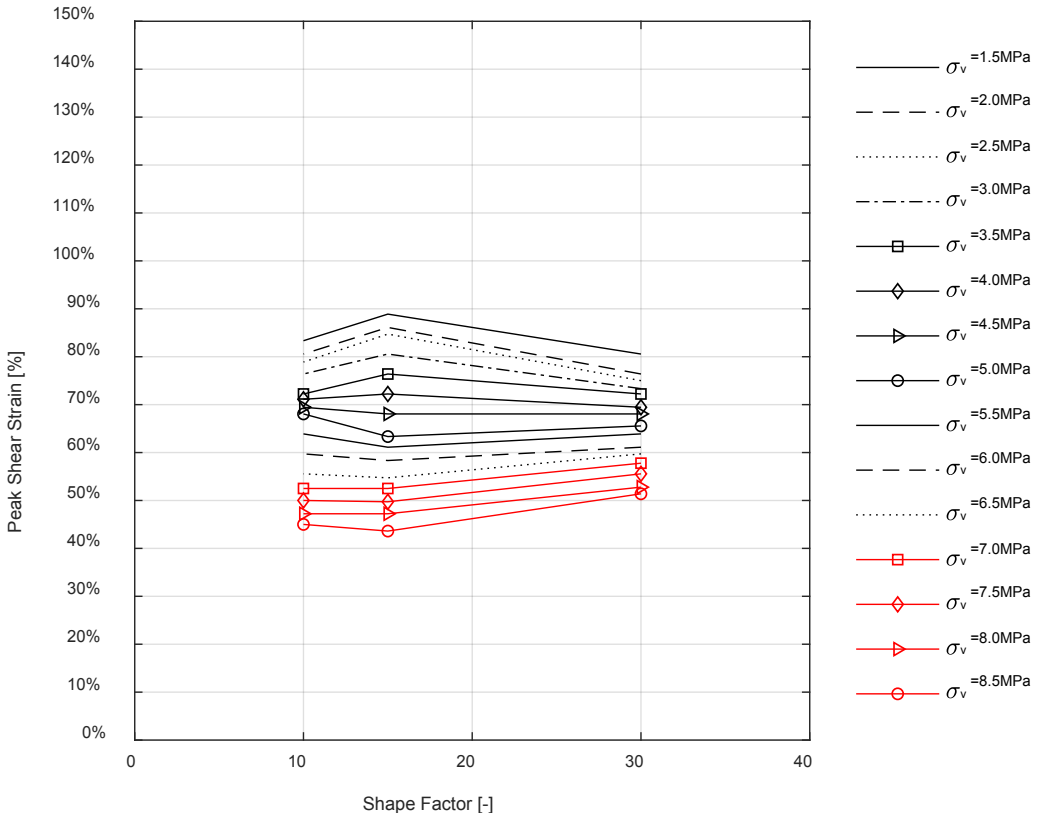


**Figure 18. Maximum Shear Strain vs. Shape Factor (B = 300 mm)**

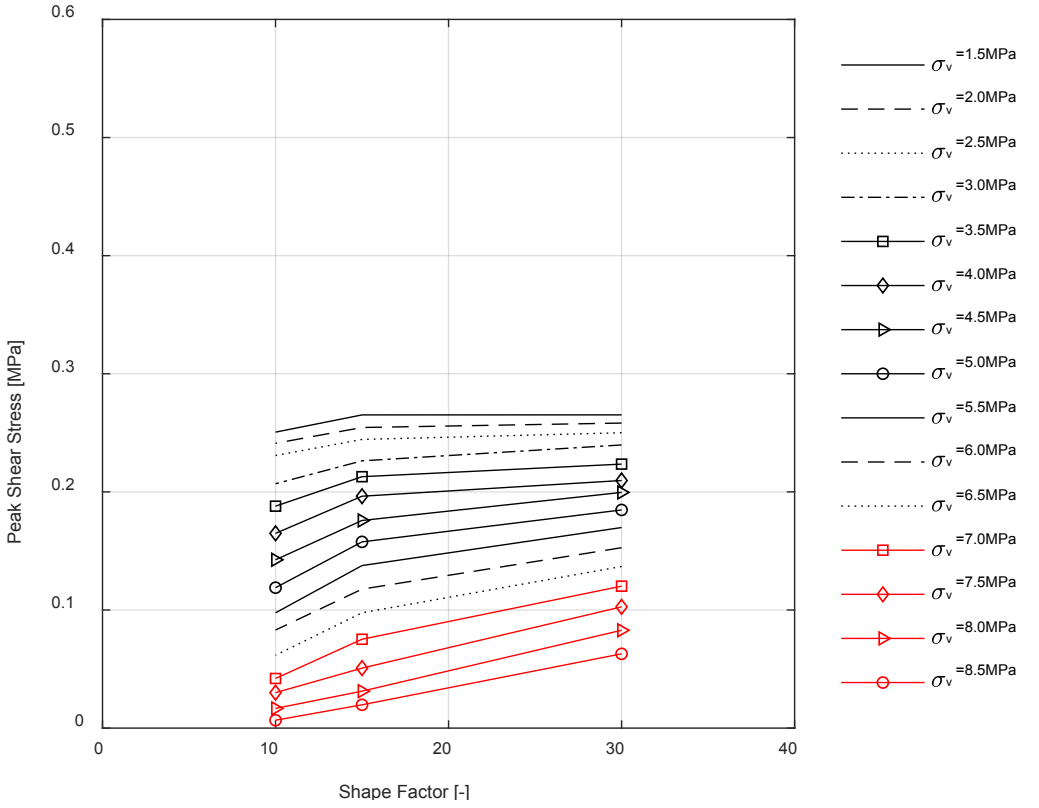


**Figure 19. Maximum Shear Stress vs. Shape Factor (B = 300 mm)**

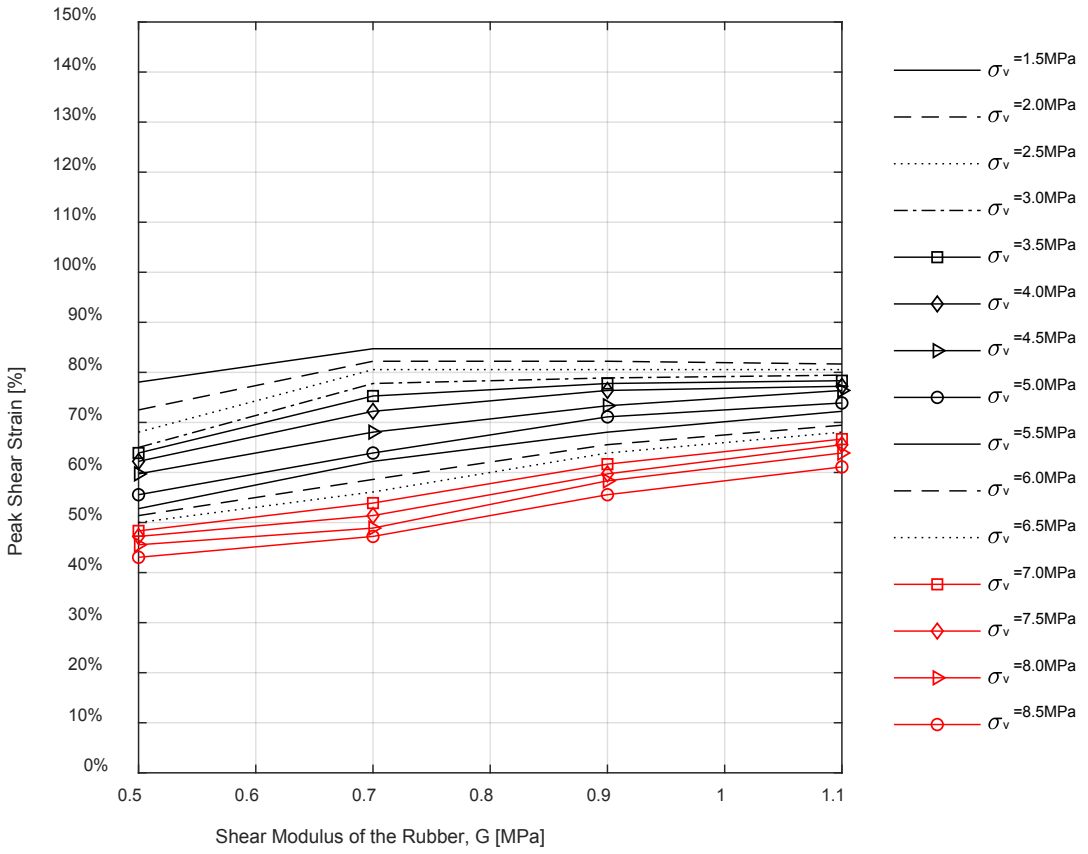


**Figure 20. Peak Shear Strain vs. Shear Modulus of the Rubber (B = 300 mm)**

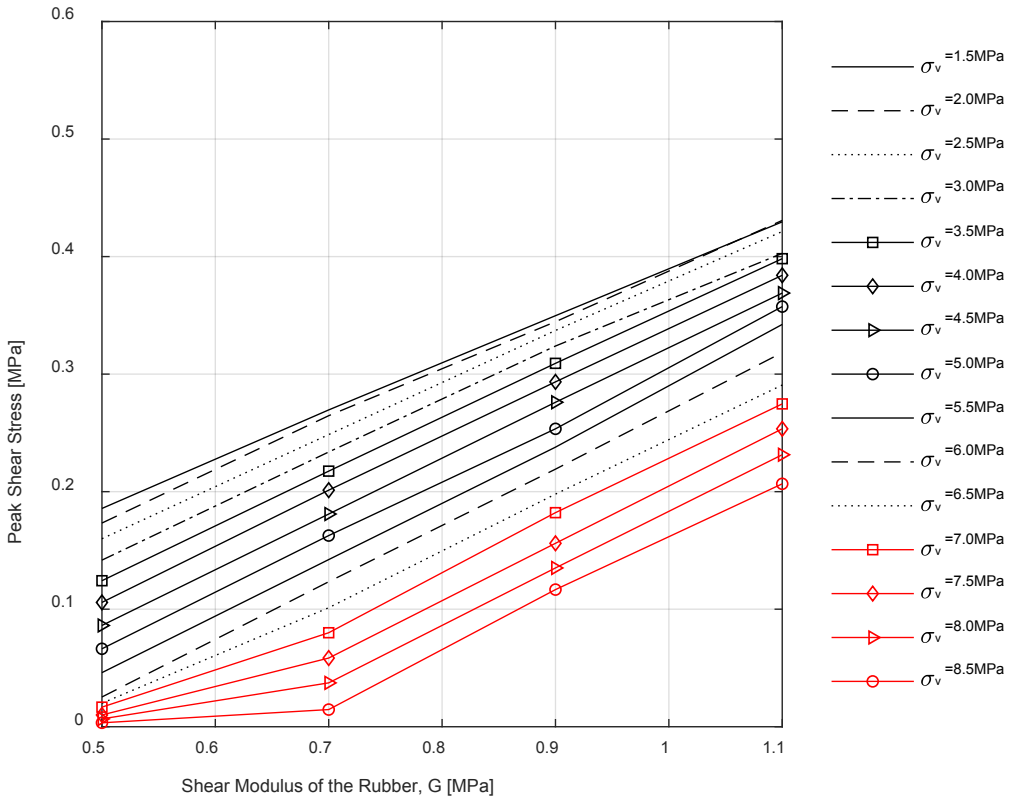


**Figure 21. Peak Shear Stress vs. Shear Modulus of the Rubber (B = 300 mm)**

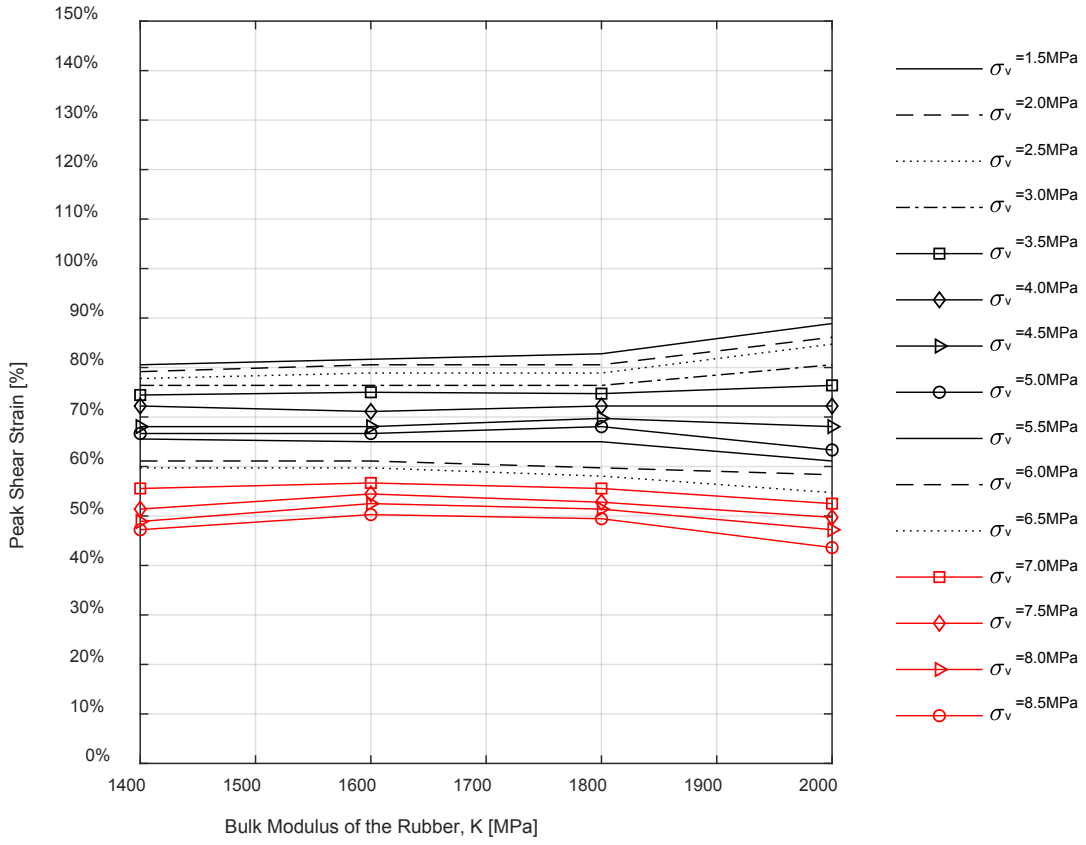


**Figure 22. Maximum Shear Strain vs. Bulk Modulus of the Rubber (B = 300 mm)**

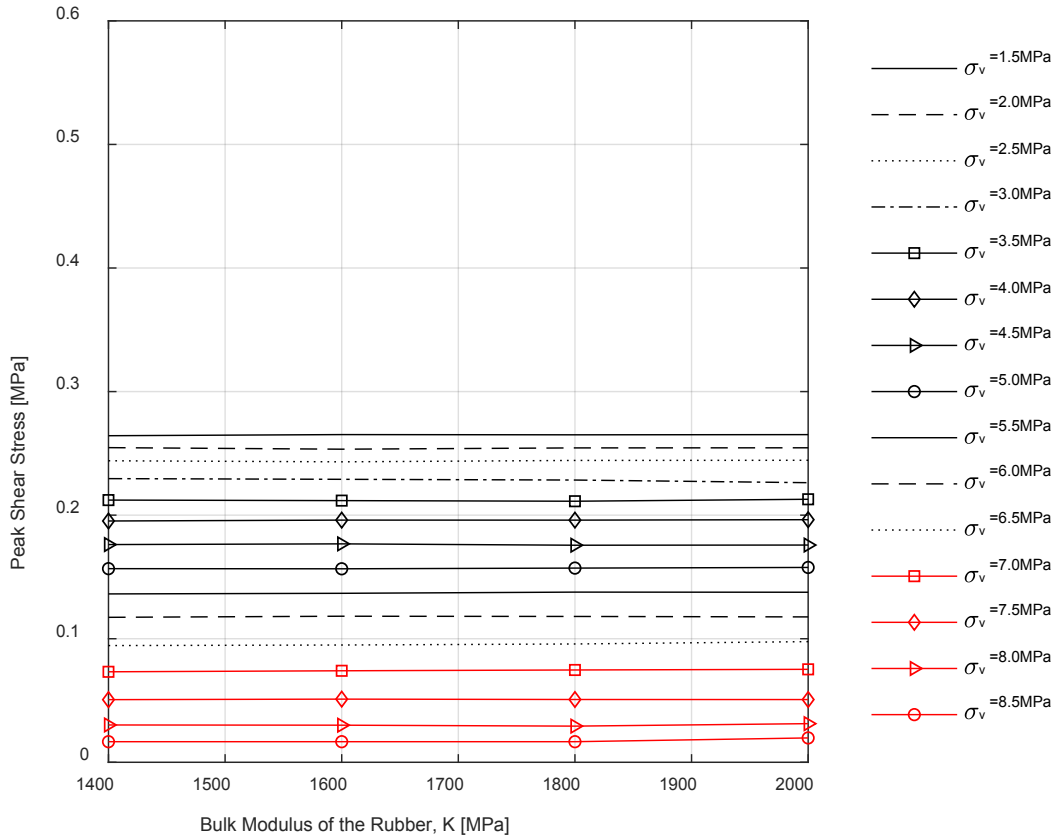


**Figure 23. Maximum Shear Stress vs. Bulk Modulus of the Rubber (B = 300 mm)**

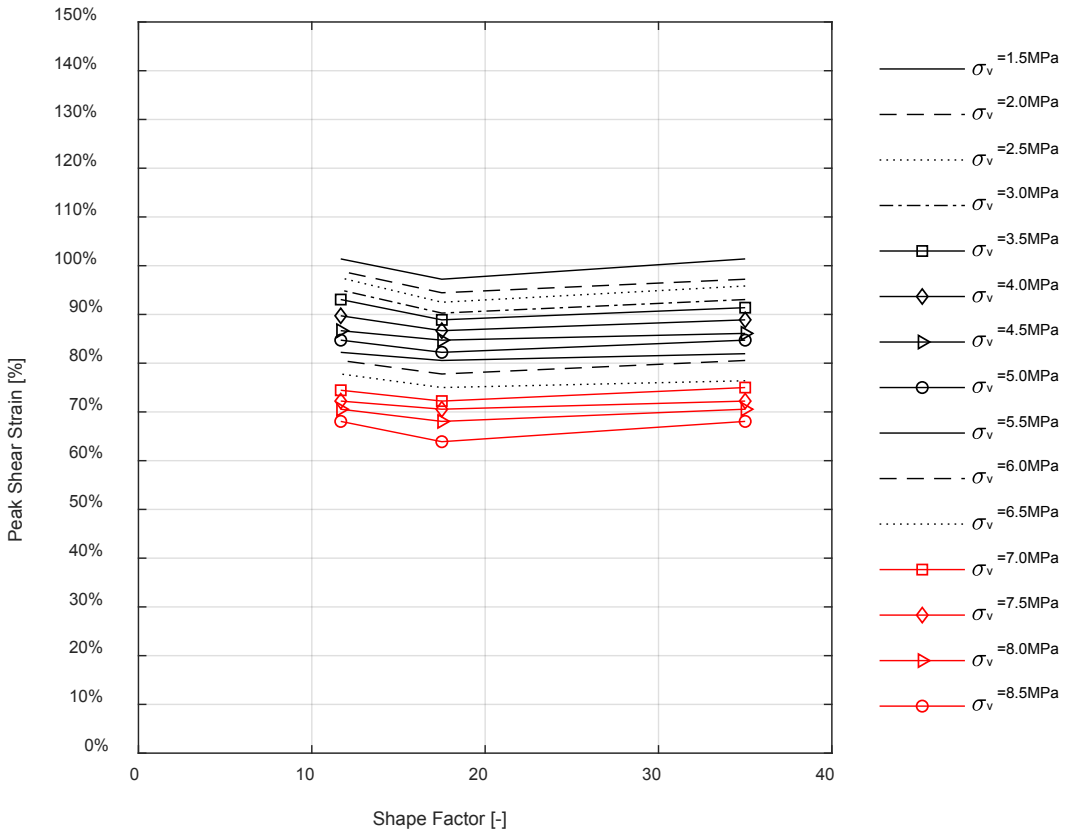


**Figure 24. Maximum Shear Strain vs. Shape Factor (B = 350 mm)**

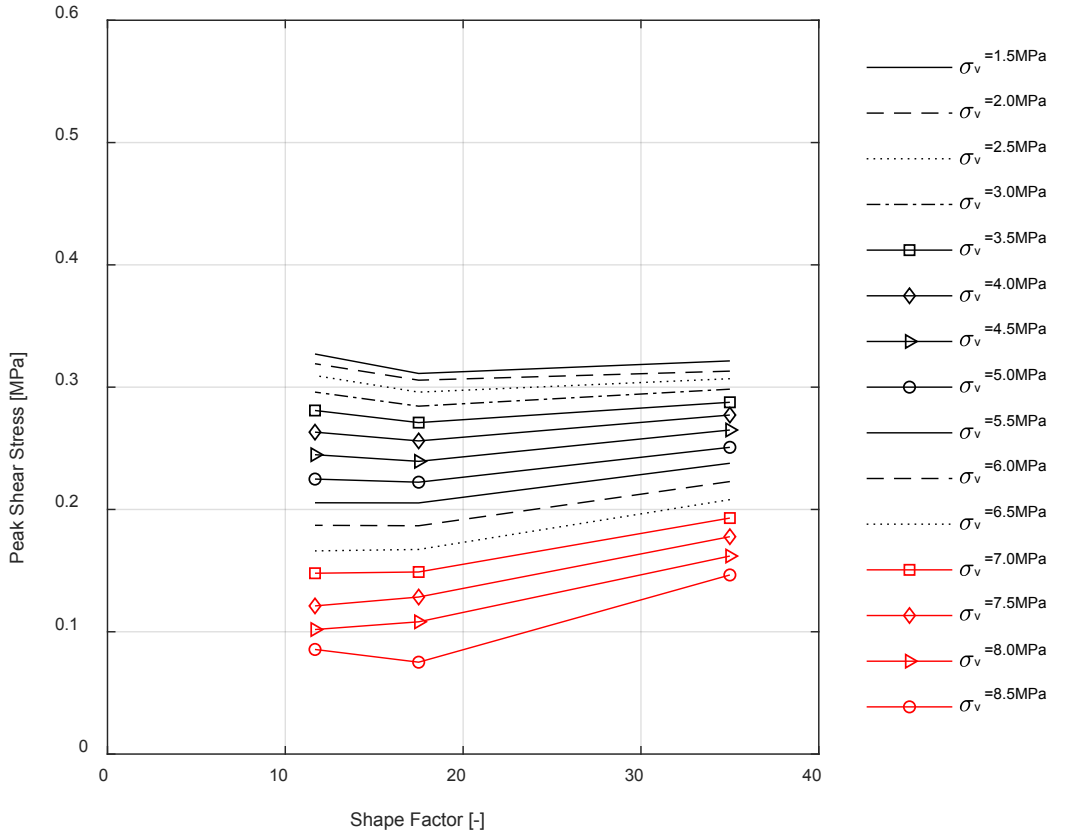


**Figure 25. Maximum Shear Stress vs. Shape Factor (B = 350 mm)**

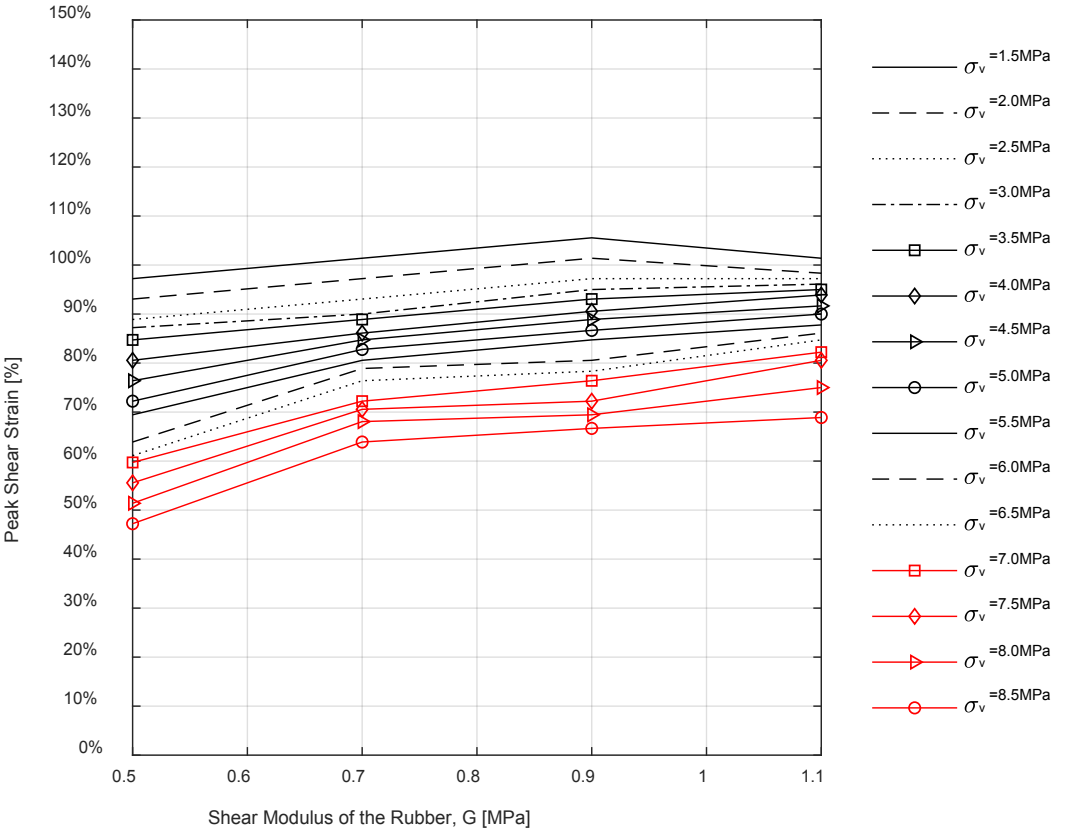


**Figure 26. Peak Shear Stress vs. Shear Modulus of the Rubber (B = 350 mm)**

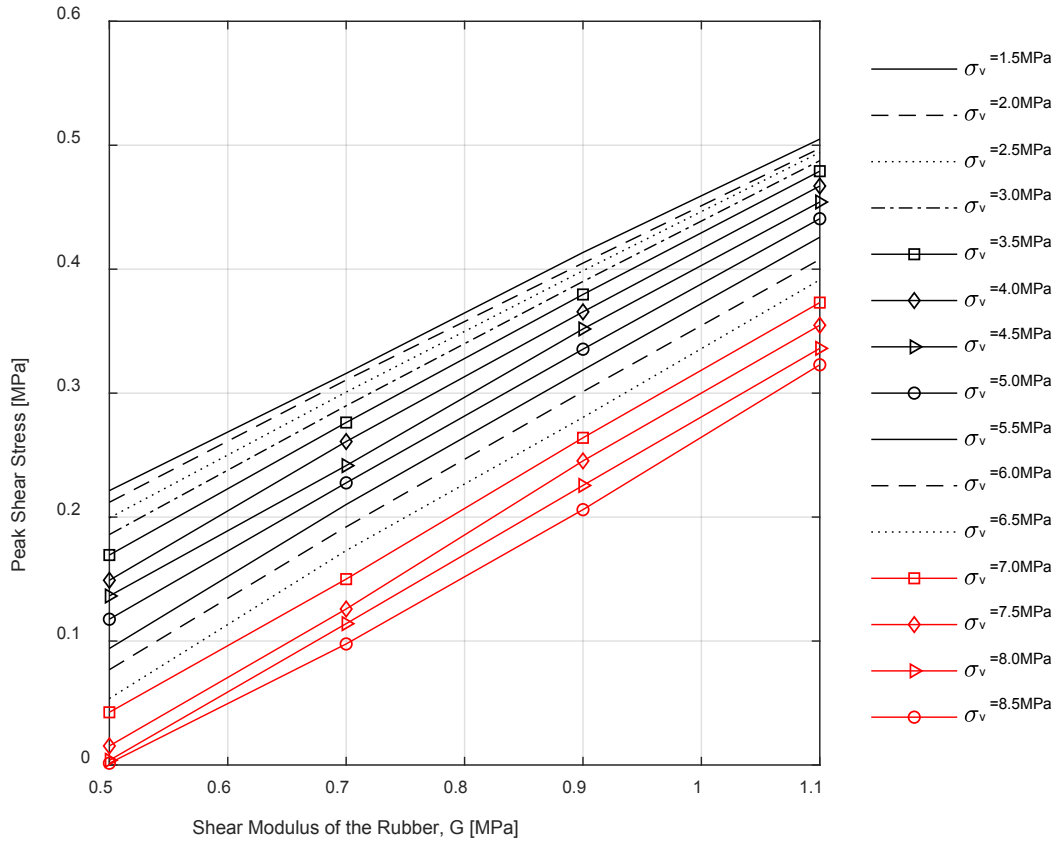


**Figure 27. Peak Shear Stress vs. Shear Modulus of the Rubber (B = 350 mm)**

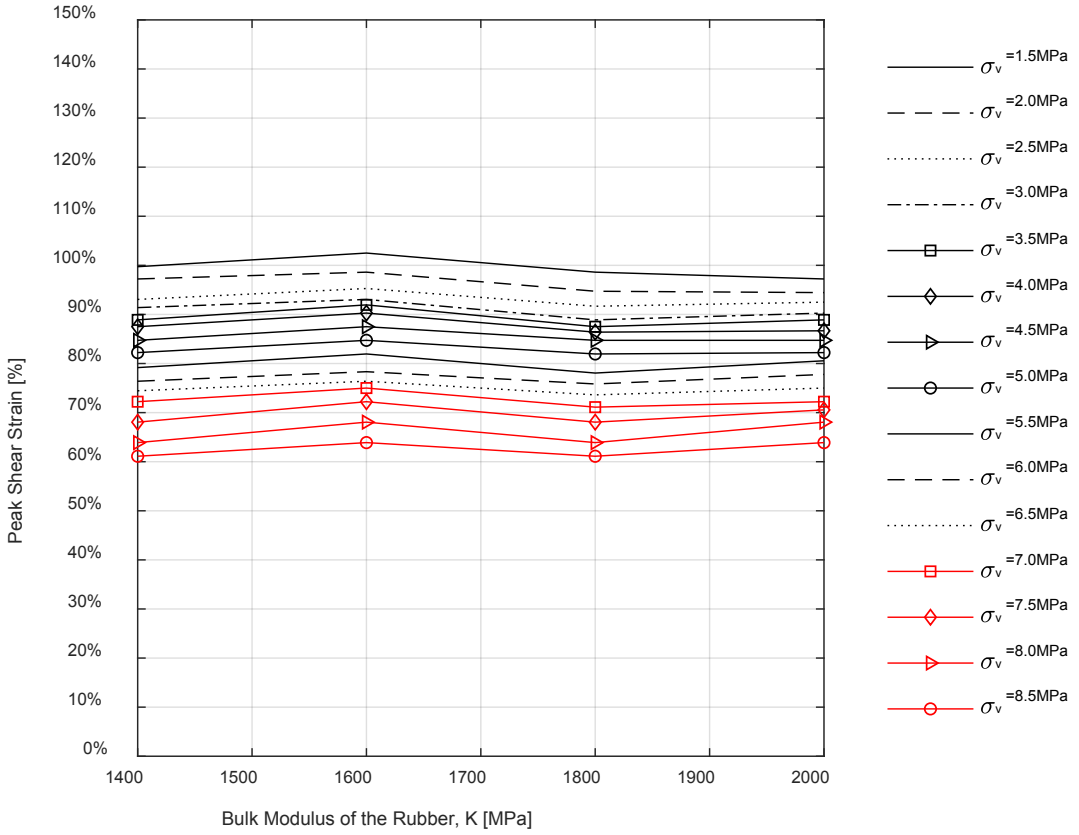


**Figure 28. Maximum Shear Strain vs. Bulk Modulus of the Rubber (B = 350 mm)**

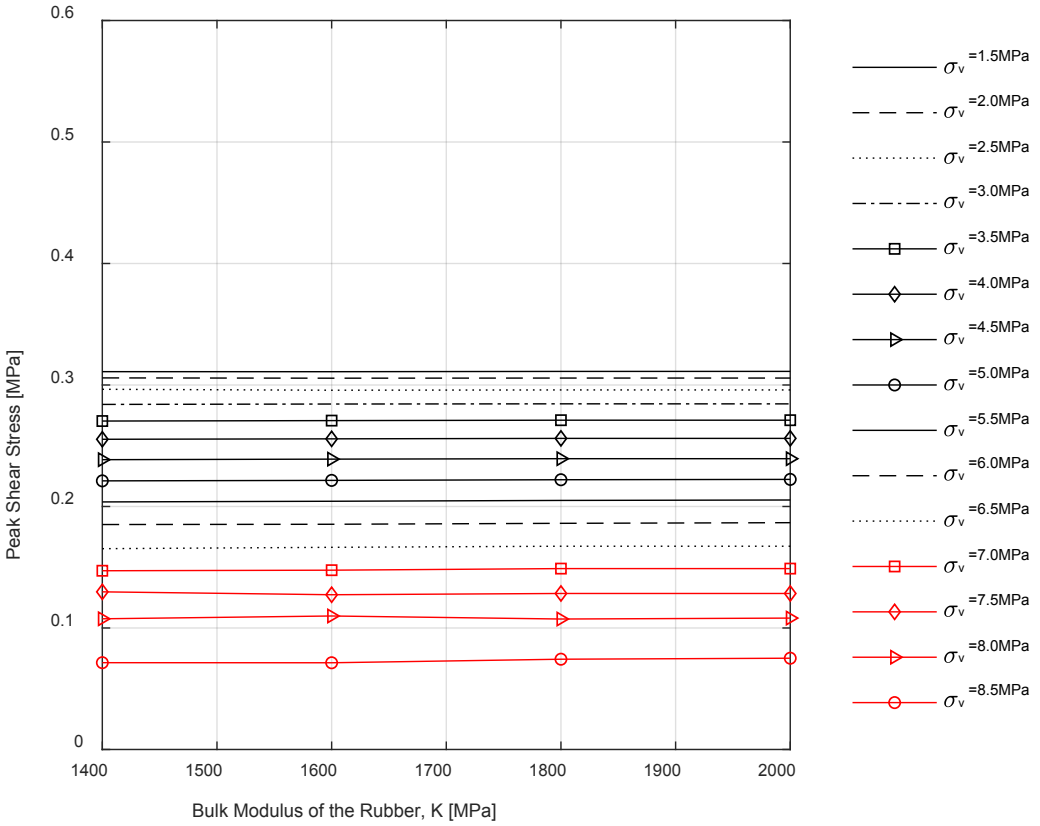


**Figure 29. Maximum Shear Stress vs. Bulk Modulus of the Rubber (B = 350 mm)**

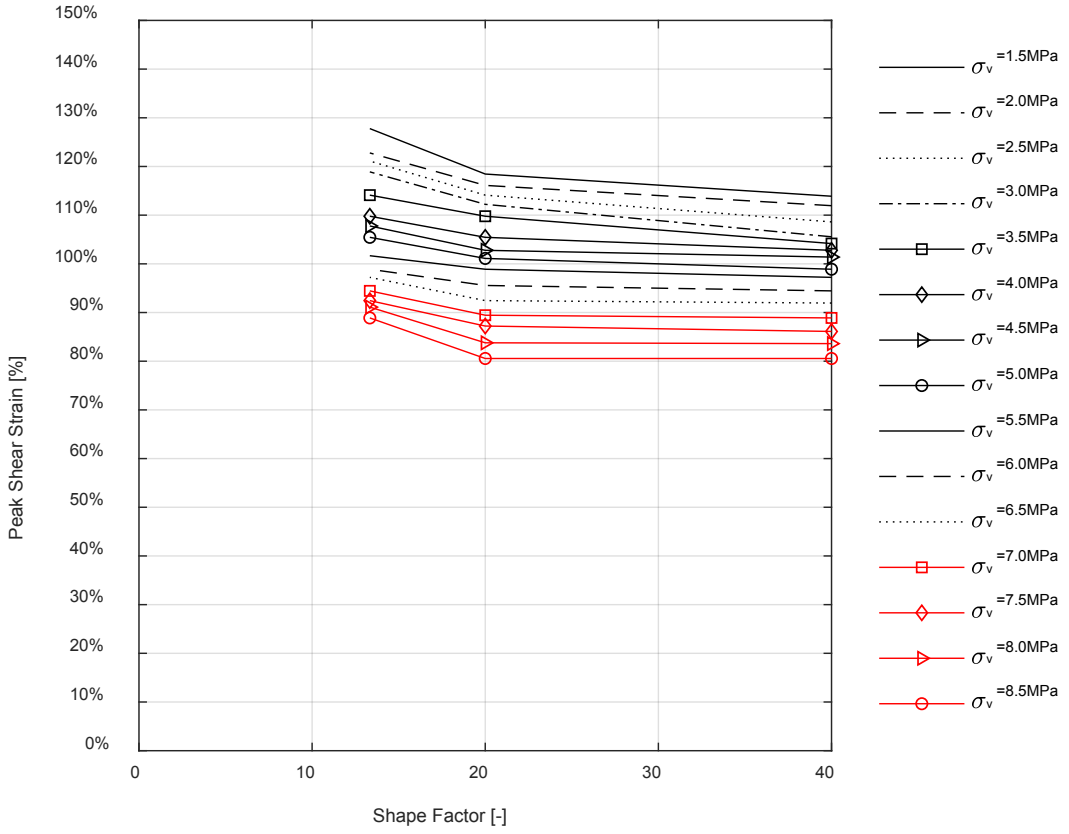


**Figure 30. Maximum Shear Strain vs. Shape Factor (B = 400 mm)**

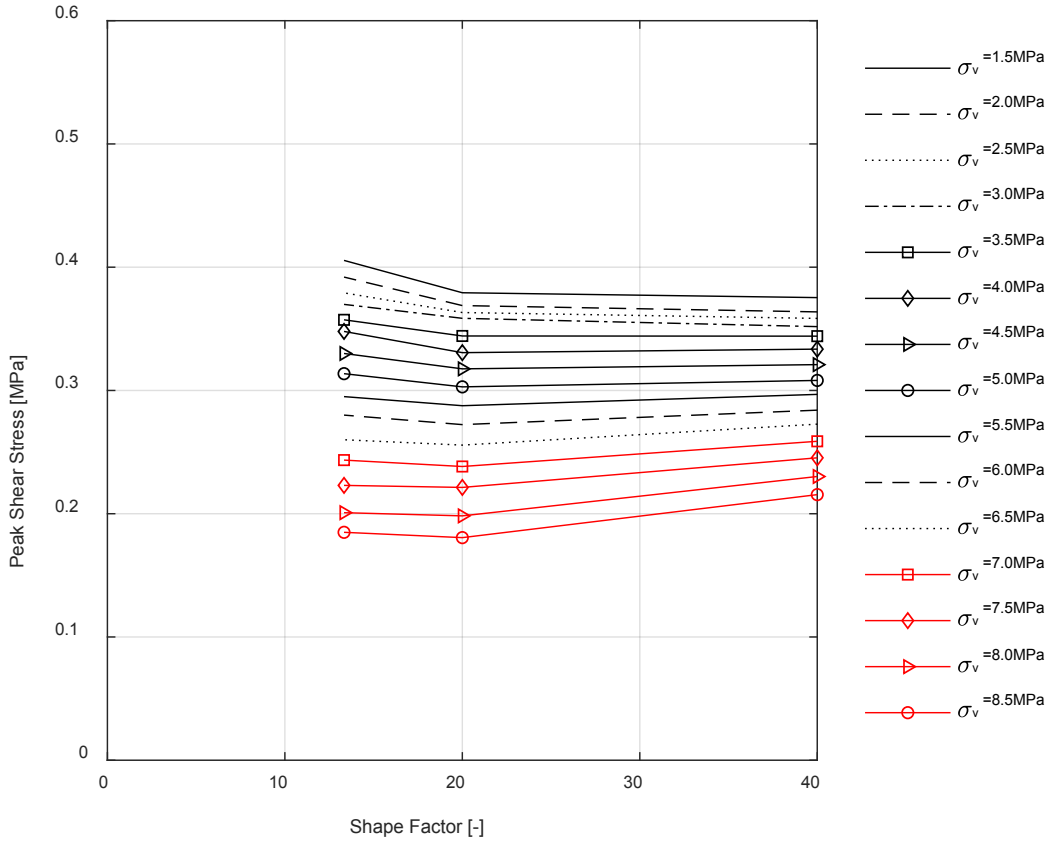


**Figure 31. Maximum Shear Stress vs. Shape Factor (B = 400 mm)**

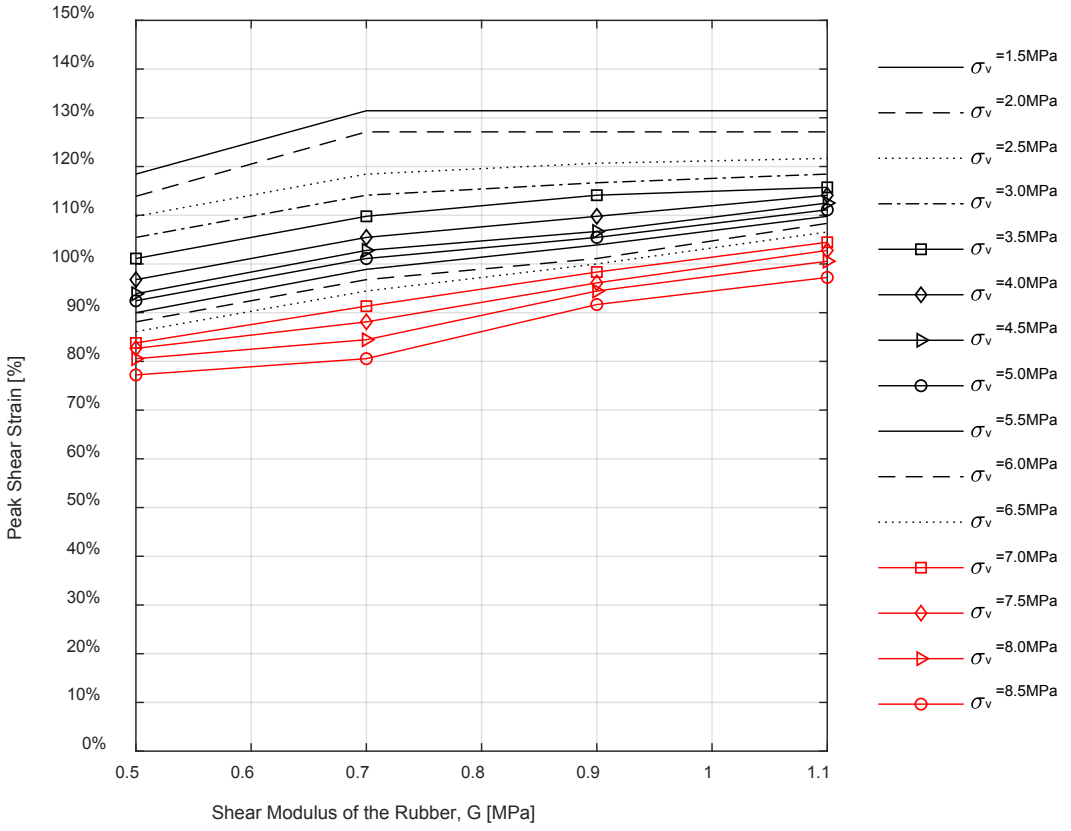


**Figure 32. Peak Shear Strain vs. Shear Modulus of the Rubber (B = 400 mm)**

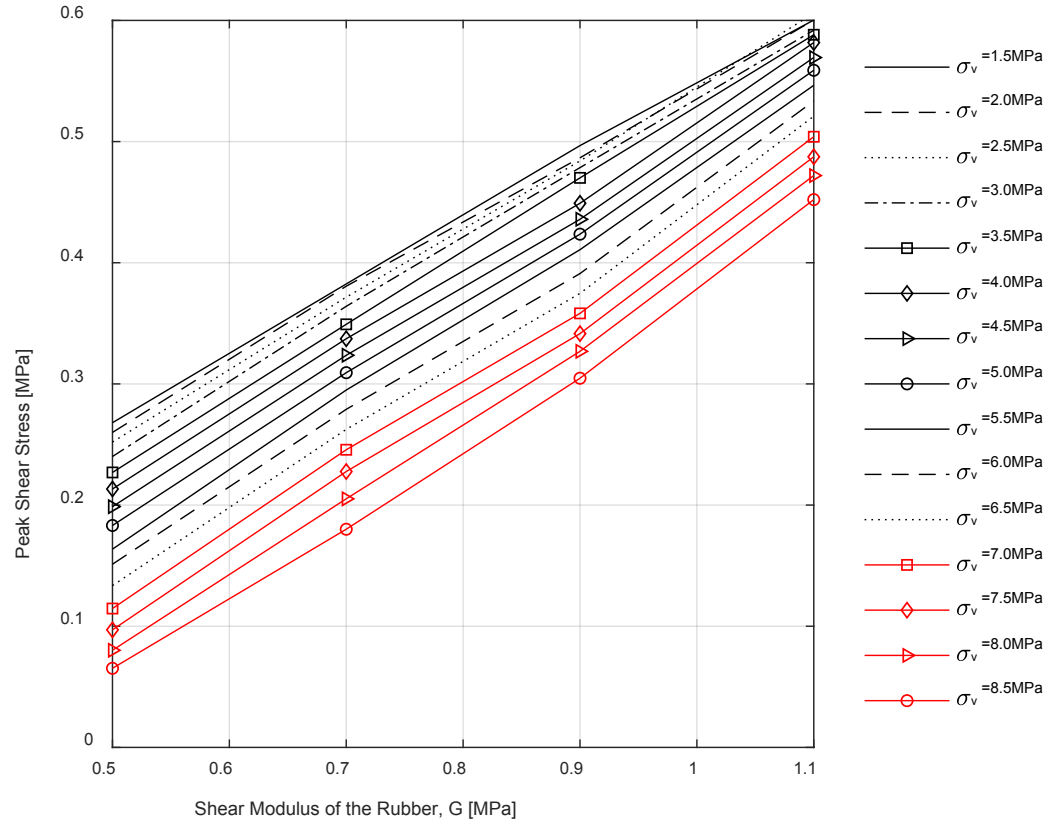


**Figure 33. Peak Shear Stress vs. Shear Modulus of the Rubber (B = 400 mm)**

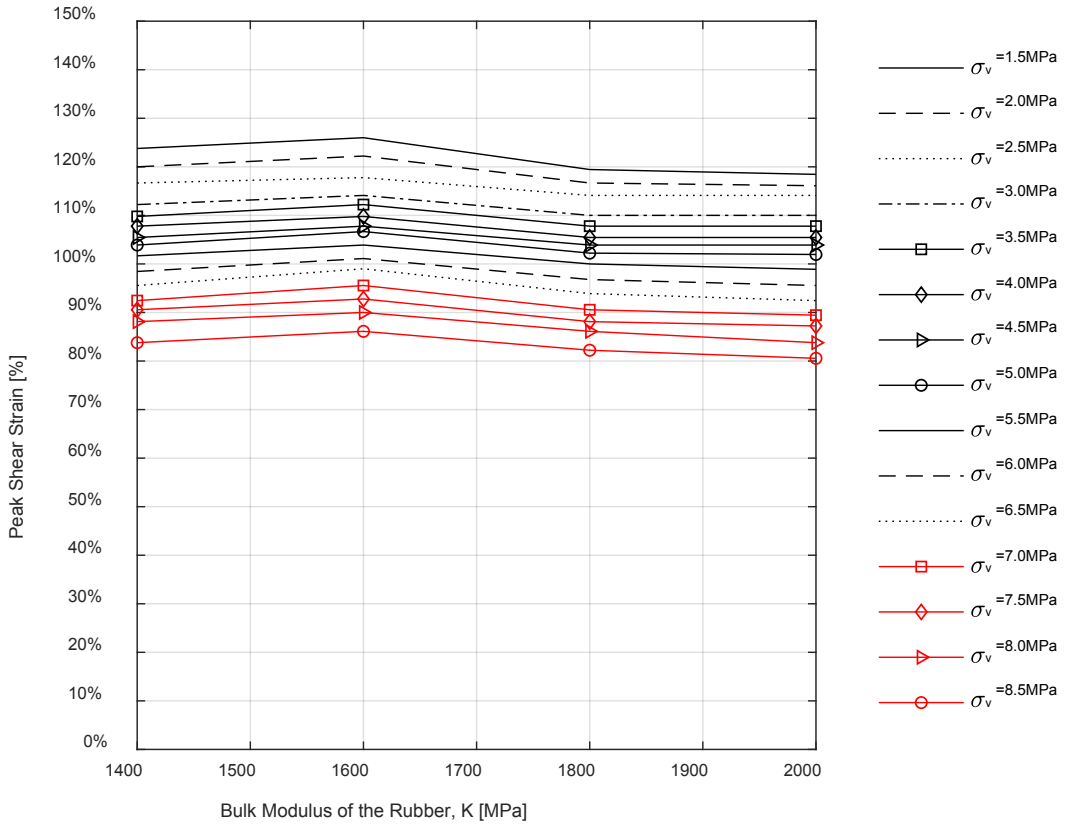


**Figure 34. Maximum Shear Strain vs. Bulk Modulus of the Rubber (B = 400 mm)**

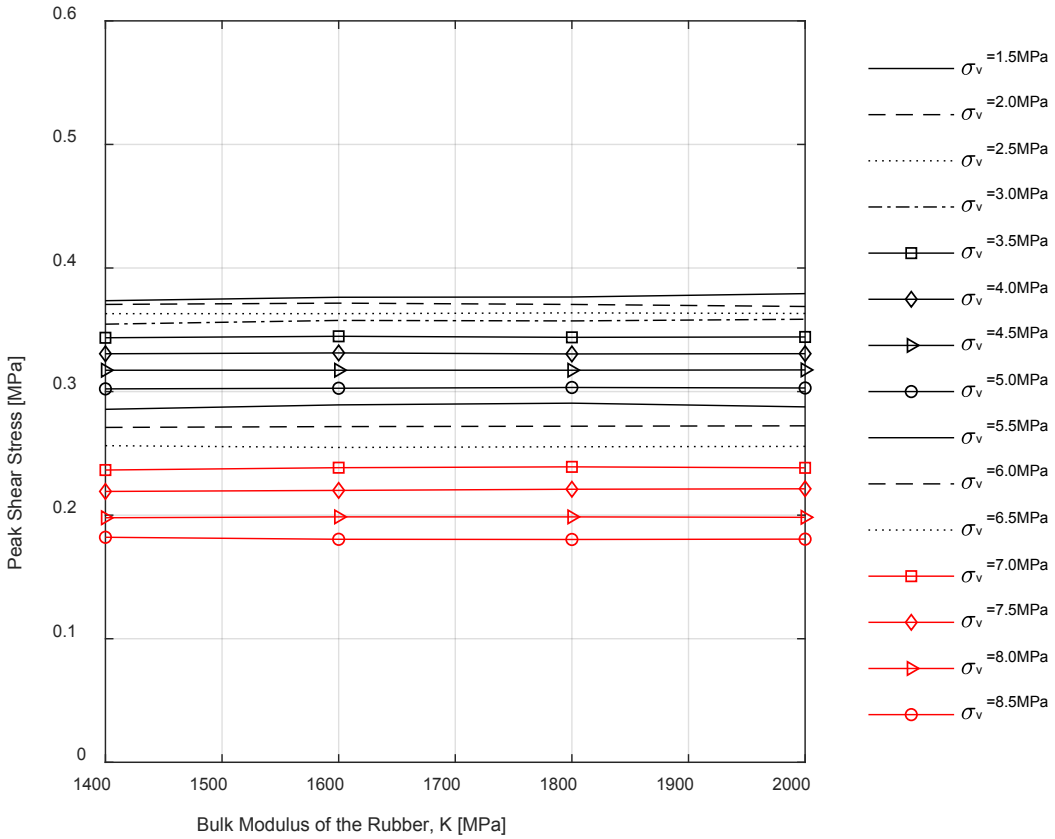


**Figure 35. Maximum Shear Stress vs. Bulk Modulus of the Rubber (B = 400 mm)**

# IV. CONCLUSIONS

This work's aims are:

(i) To investigate the stability of fiber-reinforced rubber bearings under gravity and lateral loads by adopting both numerical and analytical methods;

(ii) To evaluate the influence of different material properties, primary and secondary bearing shape factors, and axial loading conditions on the lateral load and displacement capacity of fiber-reinforced devices.

From the results of an extensive series of FEAs, the following assertions can be made:

(i) As expected, an increase of the vertical pressure on an FRB produces a reduction of the peak shear deformation capacity, independently of the aspect ratio;

(ii) The magnitude of the axial pressure modifies the maximum horizontal displacement capacity of the bearings. This modification is nonlinear with the shape factor, and the type of nonlinearity differs for lightly loaded bearings compared to heavily loaded ones;

(iii) The peak strain and stress capacity of the bearings increases with the shear modulus of the rubber while being independent of the bulk modulus of the elastomer.

The results of this study help shed some light on the response of strip-type isolators. The effects of the geometry and the shape of FRBs on their axial and lateral response merit further investigation. Furthermore, the study of bearings of different sizes and shapes should be based on 3D models of FRBs. Bearings of square and circular shape should be studied.

# ABBREVIATIONS AND ACRONYMS

| | |
|---|---|
| FE | Finite Element |
| FEA | Finite Element Analysis |
| FEM | Finite Element Method |
| FRB | Fiber Reinforced Bearing |
| GAR | Global Adaptive Remeshing |
| LRB | Laminated Rubber Bearing |

# ENDNOTES


1. E. Tubaldi, S.A. Mitoulis, and H. Ahmadi, "Comparison of Different Models for High Damping Rubber Bearings in Seismically Isolated Bridges," *Soil Dynamics and Earthquake Engineering* 104 (2018): 329–345, ISSN 0267-7261, https://doi.org/10.1016/j.soildyn.2017.09.017.

2. J.M. Kelly, "Analysis of Fiber-Reinforced Elastomeric Isolator," *Journal of Seismology and Earthquake Engineering,* 2 (1999): 19–34.

3. P.M. Osgooei, D. Konstantinidis, and M.J. Tait, "Variation of the Vertical Stiffness of Strip-Shaped Fiber-Reinforced Elastomeric Isolators Under Lateral Loading," *Composite Structures* 144 (2016): 177–184.

4. N.C. Van Engelen, P.M. Osgooei, M.J. Tait, and D. Kostantinidis, "Experimental and Finite Element Study on the Compression Properties of Modified Rectangular Fiber-Reinforced Elastomeric Isolators (MR-FREIs)," *Engineering Structures* 74 (2014): 52–64.

5. J.M. Kelly and A. Calabrese, "Mechanics of Fiber Reinforced Bearings," PEER 2012/101, 2012.

6. M. Spizzuoco, A. Calabrese, and G. Serino, "Innovative Low-Cost Recycled Rubber-Fiber Reinforced Isolator: Experimental Tests and Finite Element Analyses," *Engineering Structures* 76 (2014): 99–111.

7. P.M. Osgooei, M.J. Tait, and D. Konstantinidis, "Finite Element Analysis of Unbonded Square Fiber-Reinforced Elastomeric Isolators (FREIs) Under Lateral Loading in Different Directions," *Composite Structures* 113 (2014): 164–173.

8. J.M. Kelly, "Analysis of the Run-In Effect in Fiber-Reinforced Isolators Under Vertical Load," *Journal of Mechanics of Materials and Structures,* 3 (7) (2008): 1383–1401.

9. G. Russo, M. Pauletta, and A. Cortesia, "A Study on Experimental Shear Behavior of Fiber-Reinforced Elastomeric Isolators with Various Fiber Layouts, Elastomers and Aging Conditions," *Engineering Structures,* 52 (2013): 422–433.

10. P.M. Osgooei, M.J. Tait, and D. Konstantinidis, "Three-Dimensional Finite Element Analysis of Circular Fiber-Reinforced Elastomeric Bearings Under Compression," *Composite Structures,* 108 (2014): 191–204.

11. B.-Y. Moon, G.-J. Kang, B.-S. Kang, and J.M. Kelly, "Design and Manufacturing of Fiber Reinforced Elastomeric Isolator for Seismic Isolation," *Journal of Materials Processing Technology* 130–131 (2002): 145–150.

12. J.M. Kelly and A. Calabrese, "Analysis of Fiber-Reinforced Elastomeric Isolators Including Stretching of Reinforcement and Compressibility of Elastomer," *Ingegneria*

*Sismica,* 30 (3) (2013): 5–16.

13. M. Pauletta, A. Cortesia, I. Pitacco, and G. Russo, “A New Bi-Linear Constitutive Shear Relationship for Unbonded Fiber-Reinforced Elastomeric Isolators (U-FREIs),” *Composite Structures,* 168 (2017): 725–738.

14. H.-C. Tsai and J.M. Kelly, “Buckling Load of Seismic Isolators Affected by Flexibility of Reinforcement,” *International Journal of Solids and Structures* 42 (1) (2005): 255–269.

15. H.-C. Tsai and J.M. Kelly, “Buckling of Short Beams with Warping Effect Included,” *International Journal of Solids and Structures,* 42 (1) (2005): 239–253.

16. H. Toopchi-Nezhad, R.G. Drysdale, and M.J. Tait, “Parametric Study on the Response of Stable Unbonded-Fiber Reinforced Elastomeric Isolators (SU-FREIs),” *Journal of Composite Materials,* 43 (15) (2009): 1569–1587.

17. M.G.P. de Raaf, M.J. Tait, and H. Toopchi-Nezhad, “Stability of Fiber-Reinforced Elastomeric Bearings in an Unbonded Application,” *Journal of Composite Materials,* 45 (18) (2011): 1873–18.

18. B. Ehsani and H. Toopchi-Nezhad, “Systematic Design of Unbonded Fiber Reinforced Elastomeric Isolators,” *Engineering Structures,* 132 (2017): 383–398.

19. Kelly, J.M., Marsico, Maria Rosaria, “Stability and Post Buckling Behavior in Nonbolted Elastomeric Isolators,” *The Journal of the Anti-Seismic Systems International Society (ASSISi),* 1-(1) (2010): 41–55

20. MSC.Software Corporation, Nonlinear Finite Element Analysis of Elastomers, Santa Ana, CA: 2000.

21. L.R. Herrmann, “Elasticity Equations for Nearly Incompressible Materials by a Variational Theorem,” *The American Institute of Aeronautics and Astronautics Journal,* 3 (1965): 1896–1900.

22. MSC.Software Corporation, MSC.Marc Mentat Release Guide, Santa Ana, CA: 2005

23. A. Calabrese, “Analytical, numerical and experimental study of a novel low-cost base isolation system,” 24 July 2013, http://www.fedoatd.unina.it/id/eprint/876.

24. J.M. Kelly and S. Takhirov, Analytical and Experimental Study of Fiber-Reinforced Strip Isolators, Report 2002-11, Pacific Earthquake Engineering Research Center, University of California, Berkeley: 1–106.

# BIBLIOGRAPHY

Calabrese, Andrea. Analytical, numerical and experimental study of a novel low-cost base isolation system. 24 July 2013. http://www.fedoatd.unina.it/id/eprint/876.

De Raaf, Michael G.P., Tait, Michael J., Toopchi-Nezhad, Hamid. “Stability of Fiber-Reinforced Elastomeric Bearings in an Unbonded Application.” *Journal of Composite Materials* 45 (18) (2011): 1873–1884.

Ehsani, Behrang, Toopchi-Nezhad, Hamid. “Systematic Design of Unbonded Fiber Reinforced Elastomeric Isolators.” *Engineering Structures* 132 (2017): 383–398.

Herrmann, L.R. “Elasticity Equations for Nearly Incompressible Materials by a Variational Theorem.” *The American Institute of Aeronautics and Astronautics Journal* 3 (1965): 1896–1900.

Kelly, James Marshall “Analysis of Fiber-Reinforced Elastomeric Isolator.” *J. Seismol. Earthquake Eng.* 2 (1999): 19–34.

Kelly, James Marshall. “Analysis of the Run-In Effect in Fiber-Reinforced Isolators Under Vertical Load.” *Journal of Mechanics of Materials and Structures,* 3 (7) (2008): 1383–1401.

Kelly, James Marshall, and Calabrese, A. “Analysis of Fiber-Reinforced Elastomeric Isolators Including Stretching of Reinforcement and Compressibility of Elastomer.” *Ingegneria Sismica,* 30 (3) (2013): 5–16.

Kelly, James Marshall, and Calabrese, Andrea. Mechanics of Fiber Reinforced Bearings. PEER 2012/101, 2012.

Kelly, James Marshall, and Marsico, Maria Rosaria. “Stability and Post Buckling Behavior in Nonbolted Elastomeric Isolators.” *The Journal of the Anti-Seismic Systems International Society (ASSISi),* (2010): 41–55.

Kelly, James Marshall, Takhirov, Shakhzod M. “Analytical and Experimental Study of Fiber-Reinforced Strip Isolators.” Report 2002-11, Pacific Earthquake Engineering Research Center, University of California, Berkeley, 2002: 1–106.

Moon, Byung-Young, Kang, Gyung-Ju, Kang, Beom-Soo, and Kelly, James Marshall “Design and Manufacturing of Fiber Reinforced Elastomeric Isolator for Seismic Isolation.” *Journal of Materials Processing Technology,* 130–131 (2002): 145–150.

MSC.Software Corporation. MSC.Marc Mentat Release Guide. Santa Ana, CA: 2005.

MSC.Software Corporation. Nonlinear Finite Element Analysis of Elastomers. Santa Ana, CA: 2000.

Osgooei, Peyman M., Konstantinidis, Dimitrios, and Tait, Michael J. “Variation of the Vertical Stiffness of Strip-Shaped Fiber-Reinforced Elastomeric Isolators Under Lateral Loading.” *Composite Structures,* 144 (2016): 177–184.

Osgooei, Peyman M., Tait, Michael J., and Konstantinidis, Dimitrios. “Finite Element Analysis of Unbonded Square Fiber-Reinforced Elastomeric Isolators (FREIs) Under Lateral Loading in Different Directions.” *Composite Structures,* 113 (2014) 164–173.

Osgooei, Peyman M., Tait, Michael J., and Konstantinidis, Dimitrios. “Three-Dimensional Finite Element Analysis of Circular Fiber-Reinforced Elastomeric Bearings Under Compression.” *Composite Structures,* 108 (2014): 191–204.

Pauletta, Margherita, Cortesia, Andrea, Pitacco, Igino, and Russo, Gaetano. “A New Bi-Linear Constitutive Shear Relationship for Unbonded Fiber-Reinforced Elastomeric Isolators (U-FREIs).” *Composite Structures,* 168 (2017):725–738.

Russo, Gaetano, Pauletta Margherita, and Cortesia, Andrea. “A study on experimental shear behavior of fiber-reinforced elastomeric isolators with various fiber layouts, elastomers and aging conditions (2013) *Engineering Structures*, 52, pp. 422–433.

Spizzuoco, Mariacristina., Calabrese, Andrea., and Serino, Giorgio. “Innovative Low-Cost Recycled Rubber-Fiber Reinforced Isolator: Experimental Tests and Finite Element Analyses.” *Engineering Structures,* 76 (2014): 99–111.

Toopchi-Nezhad, Hamid, Drysdale, Robert G., and Tait, Michael J. “Parametric Study on the Response of Stable Unbonded-Fiber Reinforced Elastomeric Isolators (SU-FREIs).” *Journal of Composite Materials,* 43 (15) (2009): 1569–1587.

Tsai, Hsiang-Chuan, and Kelly, James Marshall. “Buckling Load of Seismic Isolators Affected by Flexibility of Reinforcement.” *International Journal of Solids and Structures,* 42 (1) (2005): 255–269.

Tsai, Hsiang-Chuan, and Kelly, James Marshall. “Buckling of Short Beams with Warping Effect Included.” *International Journal of Solids and Structures,* 42 (1) (2005): 239–253.

Tubaldi, Enrico, Mitoulis, Stergios A., and Ahmadi, Hamid R. “Comparison of Different Models for High Damping Rubber Bearings in Seismically Isolated Bridges.” *Soil Dynamics and Earthquake Engineering,* 104 (2018): 329–345, ISSN 0267-7261, https://doi.org/10.1016/j.soildyn.2017.09.017.

Van Engelen, Neil C., Osgooei Peyman M., Tait, Michael J., and Kostantinidis, Dimitrios “Experimental and Finite Element Study on the Compression Properties of Modified Rectangular Fiber-Reinforced Elastomeric Isolators (MR-FREIs).” *Engineering Structures,* 74 (2014): 52–64.

# ABOUT THE AUTHORS

## ANDREA CALABRESE, PHD, ING, CENG, MICE

Dr. Calabrese joined the California State University Long Beach, Civil Engineering and Construction Engineering Management (CECEM) Department as an Assistant Professor in Fall 2017. He gained a PhD in Construction Engineering with an emphasis in Structural Engineering in 2013. He was a visiting research fellow at the Pacific Earthquake Engineering Research Center (PEER) from 2010–2012 along with having been a postdoctoral researcher of the ReLUIS Consortium at the Italian Network of University Laboratories in Earthquake Engineering from 2013–2014. Dr. Calabrese has worked as a Structural Engineer at Foster & Partners (London and Italy) for seven years. He has been a registered engineer in Italy since 2009 and a Chartered Engineer (CEng) and Full Member of the Institution of Civil Engineers (MICE) in the UK since 2017. Dr. Calabrese's current research interests are in the fields of experimental testing, structural dynamics, base isolation, vibration engineering, and the development of novel low-cost devices for the seismic protection of buildings. He has carried out numerous large-scale experimental studies of base isolation systems and energy-absorbing devices on the shaking table at the Department of Structural Engineering at the University of Naples in Italy. This work has been instrumental in developing low-cost seismic isolation systems using recycled rubber and flexible reinforcements for the seismic protection of buildings in developing regions.

## SIMONE GALANO, VISITING SCHOLAR

Simone Galano is a PhD student from the University of Naples Federico II, Italy. He is currently working at the CSULB CECEM Department on a portion of the research studies for his doctoral thesis. His responsibilities included the preparation of the research report.

## NGHIEM TRAN , RESEARCH ASSISTANT

Nghiem Tran is an undergraduate student at the CSULB CECEM Department. His responsibilities included performing this study's Finite Element Analyses.

# PEER REVIEW

San José State University, of the California State University system, and the Mineta Transportation Institute (MTI) Board of Trustees have agreed upon a peer review process required for all research published by MTI. The purpose of the review process is to ensure that the results presented are based upon a professionally acceptable research protocol.

# MTI FOUNDER

## Hon. Norman Y. Mineta

# MTI BOARD OF TRUSTEES



## Directors



## Research Associates Policy Oversight Committee



MINETA TRANSPORTATION INSTITUTE